The long noncoding RNA ADIPINT is a gatekeeper of pyruvate carboxylase function regulating human fat cell metabolism

Alastair Kerr
Karolinska Institutet https://orcid.org/0000-0003-2085-1542
Kelvin Kwok
Karolinska Institute
Alison Ludzki
Karolinska Institutet
Dominique Langin
Institut National de la Santé et de la Recherche Médicale (Inserm), UMR1048, Institute of Metabolic and Cardiovascular Diseases, https://orcid.org/0000-0002-2669-7825
Ingrid Dahlman
Karolinska Institute
Peter Arner
Karolinska Institute https://orcid.org/0000-0002-6208-6220
Hui Gao (Hui.Gao@ki.se)
Karolinska Institute

Article

Keywords:

Posted Date: May 5th, 2021

DOI: https://doi.org/10.21203/rs.3.rs-83614/v1

Version of Record: A version of this preprint was published at Nature Communications on May 26th, 2022. See the published version at https://doi.org/10.1038/s41467-022-30620-0.

The long noncoding RNA ADIPINT is a gatekeeper of pyruvate carboxylase function regulating human fat cell metabolism

Kerr A G[1], Wang Z[2], Kwok K H M[1,3], Langin D[4,5], Bergo M O[3], Ludzki A[1], Dahlman I[1], Mim C[2,], Arner P[1], Gao H[3]

1. Lipid Laboratory, Department of Medicine (H7), Karolinska Institutet, Huddinge 141 86, Sweden
2. Dept. for Biomedical Engineering and Health Systems, Royal Technical Institute, Sweden
3. Department of Biosciences and Nutrition, Karolinska Institutet, Huddinge, 141 83, Sweden
4. Institute of Metabolic and Cardiovascular Diseases (I2MC),Institut National de la Santé et de la Recherche Médicale (Inserm), Université de Toulouse, UPS, UMR1297, Toulouse, France
5. Department of Biochemistry, Toulouse University Hospitals, CHU Toulouse, France

Lead contact: AKG, alastair.kerr@ki.se

Corresponding authors: PA, peter.arner@ki.se and HG, hui.gao@ki.se

Abstract

The pleiotrophic function of long noncoding RNAs (lncRNAs) is well recognized, but their direct role in regulating metabolic homeostasis is less understood. Here, we describe a human adipocyte-specific lncRNA, ADIPINT, which regulates pyruvate carboxylase (PC) an enzyme pivotal to lipid/carbohydrate metabolism. With a novel approach, Targeted RNA-protein identification using Orthogonal Organic Phase Separation (TROOPS), we show that ADIPINT binds to PC *in vivo*. ADIPINT knockdown alters the mitochondrial interactome of the enzyme leading to reduced activity. Decreases in ADIPINT levels reduces adipocyte lipid synthesis and breakdown as well as cellular bioenergetics. In human white adipose tissue, ADIPINT expression is increased in obesity and linked to insulin resistance. Changes in ADIPINT expression tightly correlate with adipose PC activity and variations in fat cell size, insulin sensitivity or the amount of adipose tissue. Thus, we identify ADIPINT as an important regulator of lipid and energy metabolism in human white adipocytes.

(148/150 words)

Introduction

Multiple disturbances in white adipose tissue (WAT) function are well described and include altered lipid metabolism and ensuing insulin resistance[1–3]. Changes in lipid synthesis and breakdown rates in fat cells govern lipid turnover, which in turn is a key regulator of fat mass[4,5]. Lipids make up more than 95% of white adipocyte volume and thus, by gaining a better understanding of factors that influence lipid metabolism and

the lipid turnover rate, key mechanisms involved in determining adipose depot size can be elucidated and novel adipose targeting treatments can be developed.

Long noncoding RNAs (lncRNAs) are a novel class of polymeric molecules which are differentially expressed in WAT during the development of metabolic diseases[6]. Compared to protein-coding genes, lncRNAs display greater cell-type specificity[7]. Thus, identifying the modes of action for dysregulated, cell-specific lncRNA, may provide insights into how metabolic disturbances occur in a cell-dependent manner and pave the way for cell specific therapeutic targets. Much of the work on lncRNAs has focused on how they regulate transcription through chromatin modifications, alter the nuclear architecture, and affect mRNA kinetics[8]. In WAT, a few adipocyte-expressed lncRNAs have been shown to regulate the transcription of lipid metabolic genes[9–11]. More recently the post-transcriptional role of lncRNAs is recognized, demonstrating their ability to act as scaffolds for cell signaling mediators[12] or facilite the phosphorylation of transcription factors[13]. In human brown-like adipocytes, the lncRNA LINC00473 was shown to interact with mitochondrial and lipid droplet proteins, thereby altering the metabolism of the cell[14].

In this study we identify a human adipocyte-specific lncRNA (CATG00000106343.1), hereafter named ADIPINT for ADIpocyte specific Pyruvate carboxylase INTeracting RNA. ADIPINT acts post-transcriptionally by binding to and regulating the interactome of pyruvate carboxylase (PC) and as a result its mitochondrial abundance and enzymatic activity. Alterations in ADIPINT expression regulate lipid and energy metabolism within fat cells. We show that pertubations in PC activity are able to cause these effects on adipocyte metabolism and that the expression of ADIPINT and PC activity are closely linked in human WAT phenotypes suggestive of a physiological role.

(340/500)

Results

Identification of ADIPINT as a potential regulator of human fat cell lipid metabolism

To discover lncRNAs involved in fat cell metabolism, we examined their WAT expression in a selected cohort of female patients with obesity, before and after undergoing marked body weight reduction by Roux-en-Y gastric bypass (RYGB) surgery. The changes in lncRNA expression were further associated with the changes

in fat mass and fat cell size, with fat cell size reflecting the net balance between synthesis and breakdown of triglycerides and influencing WAT insulin sensitivity[15]. Clinical characteristics of the cohort are given in Supplementary Table 1 and have been reported previously[16,17]. Compared to pre-surgery, 760 lncRNA were differentially regulated at two-years follow-up when there was on average a 32% decrease in body weight and substantial decreases in fat mass and fat cell size (Fig. 1a and Supplementary Table 2). To prioritize candidates genes for further investigation, the aforementioned lncRNAs were compared with 67 lncRNAs previously found to be differentially expressed in WAT of insulin sensitive compared to insulin resistant women with obesity[9]. Twelve lncRNAs displayed a significant concordant change in both clinical cohorts (i.e. higher expression before RYGB and in the insulin resistant state; or lower expression two years post-RYGB and in the insulin-sensitive state) (Fig. 1a and Supplementary Table 3). ADIPINT (CATG00000106343.1) displayed the greatest fold change in both cohorts of the twelve genes and the second largest fold change of all lncRNAs two years post-RYGB (Fig. 1a). In addition, the changes in total fat mass and adipocyte cell volume correlated positively with the change in ADIPINT expression post-RYGB (Fig. 1b). These data suggests that ADIPINT is a promising candidate and further study was devoted to this lncRNA.

ADIPINT is intergenic and located on chromosome 9 (Fig. 1c). None of the three transcripts in the ADIPINT loci have protein coding potential according to CPAT, RNACode, phyloCSF, and sORF riboseq coding prediction softwares. ADIPINT is not conserved between phylogenetically distant species at the sequence or genome synteny level. RNA-seq and CAGE-seq[18] in human adipose-derived stem cells (hADSC) from subcutaneous WAT revealed that transcript 2 of ADIPINT is the dominant isoform expressed in mature adipocytes (Fig. 1c). Transcript 2 is 4.8 kb long and contains two exons (Fig. 1c); the junction was validated by qPCR and Sanger sequencing (data not shown). Upregulation of ADIPINT expression during differentiation in hADSC and enrichment in mature adipocytes isolated from WAT were confirmed by qRT-PCR (Fig. 1d,e). Analysis of RNA expression in different human cell types in the FANTOM5[7] database demonstrated that ADIPINT is exclusively expressed in adipocytes (Fig 1f). Subcellular fractionation studies and RNA-fluorescence in situ hybridization (FISH) revealed ADIPINT to be predominantly localized in the cytoplasm of adipocytes (Fig. 1g-h). Thus, ADIPINT is an adipocyte-specific cytoplasmic lncRNA linked to insulin resistance, fat mass, adipocyte size and thereby lipid metabolism.

ADIPINT expression regulates fat cell lipid metabolism

The role of ADIPINT in regulating adipocyte function was assessed by knockdown experiments in *in vitro*–differentiated hADSCs. We used three different anti-sense oligonucleotides (GapmeRs) and found that they reduced APIPINT expression by 89–97% compared to a negative control GapmeR (GapmeR NC) (Fig. 2a). ADIPINT knockdown reduced glycerol release (lipolysis index) by 27–58% (Fig. 2b); total intracellular triglyceride content by 40–66% (Fig. 2c), and insulin-stimulated lipid synthesis by 54–67% (Fig. 2d). The rate of lipid metabolism is linked to mitochondrial energy supply[19] , citrate production and the TCA cycle[20]. Therefore, we argued that the effects of ADIPINT on lipid metabolism might influence fat cell energy metabolism. Indeed, ADIPINT knockdown in adipocytes reduced the basal oxygen consumption rate (OCR) (Fig 2e, Extended Data Fig 1a), the ATP-linked OCR (Fig 2f, Extended Data Fig 1a) determined after oligomycin administration, and the extracellular acidification rate (ECAR) (Fig 2g, Extended Data Fig 1b). Therefore, ADIPINT knockdown affects both the aerobic and anaerobic respiration rates and results in impaired adipocyte lipid metabolism.

As a first step to identify the molecular action of ADIPINT, we carried out transcriptomic and proteomic analyses after knockdown with each of the three ADIPINT targeting GapmeRs. The median fold-changes induced by the three GapmeRs at the RNA and protein level correlated significantly ($r^2 = 0.2284$, p-value < 0.0001; Fig. 2h, Supplementary Tables 4-5). The downregulated mRNAs were enriched for metabolic pathways including 'pyruvate metabolism' and 'fatty acid metabolism' (Fig. 2i, Supplementary Tables 6-7). The proteome analysis revealed that 10 proteins were up- and 28 downregulated by each of the three GapmeRs independently (Supplementary Table 8). Interestingly, 19 of the 38 dysregulated proteins (marked by an asterisk in Fig 2j) were not significantly regulated at the transcript level, indicating a post-transcriptional regulation. Pathway analysis of the 38 dysregulated proteins showed overrepresentation for the GO terms 'mitochondrial matrix' and 'fatty acid metabolic process' (Supplementary Table 9-10) in line with the changes observed above in the lipid metabolism and bioenergetics analyses. Based on information at www.genecards.org, we visualized all 38 proteins affected after ADIPINT knockdown in Fig. 2j. Most proteins were downregulated and involved in fatty acid synthesis and oxidation. Proteins within the pyruvate dehydrogenase complex were downregulated as well as Aldolase A which is involved in the early steps of

glycolysis, while Pyruvate kinase isozymes R/L, involved in synthesizing pyruvate, was upregulated. Together these data indicate a clear metabolic effect of ADIPINT on lipid and energy metabolism including the regulation of key components in the mitochondria.

ADIPINT interacts with pyruvate carboxylase

As the next step to understand the mechanism by which ADIPINT regulates adipocyte metabolism, we identified its direct protein interaction partners. Previous methods to investigate lncRNA-protein binding[21,22], require large numbers of cells. Recently, orthogonal organic phase separation (OOPS)[23] enabled the non-targeted isolation of the entire RNA-bound proteome. We applied OOPS to enrich the RNA-bound proteome and then performed targeted pulldown of a specific RNA in human white adipocytes. We named this novel method Targeted RNA-protein identification using OOPS (TROOPS, see Methods for details). Adipocytes underwent UV crosslinking, followed by Trizol-chloroform extraction, where RNA-protein complexes migrate to the interphase and unbound RNA, protein and DNA in other fractions can be removed (Fig. 3a). The interphase is cleaned, sonicated and used for targeted pulldown of ADIPINT with short antisense oligonucleotides. After UV crosslinking, ADIPINT became enriched at the interphase, indicating its binding to a protein partner (Extended Data Fig. 2). Using two distinct sets of oligonucleotides, each tiled along ADIPINT, we enriched the lncRNA 3.5-4.8 fold compared to the input material (Fig. 3b). No ADIPINT expression was detected after pulldown using probes targeting Lac Z mRNA or using the ADIPINT-targeting probes with RNase. Mass-spectrometry analyses revealed that pyruvate carboxylase (PC) was significantly enriched with ADIPINT pulldown (Fig. 3c). No differences in PC abundance were found in the RNase-treated or Lac Z probe sets. All detected proteins in each experiment are listed in Supplementary Table 11. We confirmed the interaction with PC by western blot analysis (Fig. 3d). GADPH, another enzyme known to bind RNA[24], was used as a control for pulldown and interaction specificity. To validate the ADIPINT interaction, we performed immunoprecipitation of PC in hADSCs. ADIPINT was enriched when compared to IgG and this enrichment was significantly higher than that of *18S*, *PC*, and *U1* RNA (Fig. 3e). We examined the specificity of the ADIPINT and PC interaction by Gel Filtration Chromatography. Both the RNA and protein could be distinguished using a Sepharose column filtration system, establishing their specific elution volumes (Extended Data Fig. 3a). When ADIPINT and PC were combined and the resulting mixture loaded, PC and

ADIPINT eluted together at the RNA elution volume (Fig. 3f, Extended Data Fig. 3b). PC when ran alone or with ADIPINT anti-sense did not elute at the RNA elution volume to any significant degree (Fig. 3f). Furthermore, we found ADIPINT and PC to exist in the same compartments within the cell after performing subcellular fractionation (Fig. 3g) for mitochondrial and cytoplasmic fractions (Extended Data Fig. 4a-b). RNA-FISH with immunofluorescence staining for ADIPINT and PC in tandem confirmed the localization overlap (Fig. 3h). Together these data suggest a physical ADIPINT-PC interaction.

ADIPINT knockdown reduces pyruvate carboxylase activity by alterating its localization and interactome

The enzymatic activity of PC increases during adipogenesis[20], which leads to increased production of oxaloacetate used in fatty-acid, glycerol and subsequent triglyceride synthesis[25]. PC expression was not altered at the protein level after ADIPINT knockdown (Fig 2e), and we therefore hypothesized that the ADIPINT-PC interaction might regulate PC's enzymatic activity. ADIPINT was knocked down using three separate GapmeRs (1-3) and PC activity was measured as the rate of conversion of pyruvate to oxaloacetate. PC activity over time (Fig. 4a) was reduced by all target GapmeRs compared to the control GapmeR (indicated by the shift to the right). The time for reaching 50% completion of the reaction was 1.6-2.7 fold greater for GapmeRs 1-3, compared to GapmeR NC (Extended Data Fig. 5). No change was seen in PC protein expression in the same experiments (Fig. 4b). Normalising the enzyme activity by protein expression, we found that PC's activity was reduced upon ADIPINT knockdown (Fig. 4c). The decrease in PC activity was accompanied by reduced levels of intracellular oxaloacetate (Fig. 4d); intracellular pyruvate levels were unaffected (Fig. 4e). Thus, lower oxaloacetate production was not the result of low substrate availability. As PC produces oxaloacetate in the mitochondrial matrix we determined if the changes in oxaloacetate was related to less PC in the mitochondria. Consistent with previous data, western blots of whole-cell lysates revealed that thetotal amount of PC within the cell did not change following ADIPINT knockdown (Fig. 4f-g). However, the amount of PC within the mitochondrial fraction decreased after knockdown (Fig 4f-h) and the activity of PC within this fraction was also reduced (Fig. 4i). Interestingly, two PC bands were detected in the input sample, but only the larger band was detected in mitochondria and the smaller band in the cytosol (Fig. 4f).

Metabolic enzymes are compartmented within the cell putting the enzyme into the proximity of sequential enzymes within the metabolic pathway and the production of its substrate[26]. When enzymes are assembled into these specific metabolic complexes the activity for that particular enzyme is also enhanced[27]. Consequently, we asked whether ADIPINT might be important for maintaining the PC interactome? We immunoprecipitated PC after ADIPINT knockdown and analyzed the changes in the interactome in the mitochondrial and cytoplasmic fractions using mass-spectrometry. The amount of PC immunoprecipiated from each fraction in GapmeR 1- and GapmeR NC-treated cells was similar, so comparisons of interacting protein abundance could be made (Supplementary Table 12). As with changes in PC localization and activity, the proteins enriched displayed greater differences after ADIPINT knockdown in the mitochondrial fraction compared with the cytosolic (Fig. 4j). We therefore focused our analyses of PC-interacting proteins on the mitochondrial fraction. All proteins displaying a $\log_2$ fold change of 5 or greater were considered significantly altered. Knockdown of ADIPINT caused the dissociation of six proteins within the glycolysis/glyceroneogenic pathway from PC, including Phosphoenolpyruvate Carboxykinase 1, the rate limiting enzyme within this pathway[28] (Fig. 4k). Malate Dehydrogenase 1 which is important for energy metabolism was also decreased in the pulldown after ADIPINT knockdown. Without ADIPINT, PC was associated with proteins involved in fatty acid oxidation, a pathway not associated with pyruvate metabolism. ADIPINT thus appears to establish a unique interactome for PC and we suggest this regulates the activity and cellular localization of the enzyme.

Chemical inhibition of pyruvate carboxylase perturbs lipid metabolism and the bioenergetic rate in fat cells

Inhibiting PC activity in mouse adipocytes reduces lipid synthesis and triglyceride accumulation[29]. To determine if a selective targeted reduction in PC activity in human fat cells could lead to the same alterations in lipid metabolism as with ADIPINT knockdown, we incubated hADSCs with the PC inhibitor oxalate[30,31]. Oxalate reduced glycerol release, intracellular triglyceride and insulin-stimulated lipid synthesis (Fig. 5a-c). At 500 μM of oxalate the reduction of lipid metabolism was similar to ADIPINT knockdown in parallel experiments using GapmeR 1. We next assessed the effect of PC inhibition on adipocyte bioenergetics. Oxalate administration reduced basal and ATP-linked OCR as well as glucose-stimulated ECAR and a similar

decrease was seen following ADIPINT knockdown (Fig 5d-f, Extended Data Fig. 6). Thus, inhibiting PC activity can reduce lipid and energy metabolism to a similar extent as ADIPINT perturbation.

ADIPINT expression correlates with adipose pyruvate carboxylase activity and clinical phenotypes

Finally, we examined a possible physiological role of ADIPINT. A correlation between ADIPINT and PC was examined in abdominal subcutaneous adipose tissue of 19 apparently healthy women (clinical data are given in Supplementary Table 13). They were subdivided according to obesity status with body mass index of 30 kg/m^2 used as the cut-off value (9 were obese). ADIPINT expression was increased in obesity in the first examined cohort (Fig. 1a), which was confirmed in this second cohort as well (Fig. 6a). PC protein expression did not differ between groups (Fig. 6b), however PC activity was higher in women with obesity (Fig. 6c). Furthermore, ADIPINT expression and PC activity were positively correlated (Fig. 6d), while no correlation between PC protein expression and ADIPINT was observed (Extended Data Fig 7). The physiological role of ADIPINT was further examined through its association with other clinical traits in this cohort. ADIPINT expression correlated positively with fasting serum insulin and plasma triglyceride levels but not with fasting plasma cholesterol (Fig. 6e-g). Also the level of in vivo insulin resistance (measured by the homeostasis assessment method) correlated positively with ADIPINT expression (Fig 6h). In agreement with the results of the cohort used in Fig.1, ADIPINT expression, in the current cohort, correlated strongly with fat cell volume and ADIPINT expression (Fig. 6i). Up to 33% of the variation in fat cell volume between subjects could be explained by variations in ADIPINT expression (i.e. adjusted r^2) (Supplementary Table 14). These data support the notion that ADIPINT is a physiological regulator of lipid storage and fat cell size at least in women.

Discussion

The recent discovery that many enzymes can bind RNA has added a new layer of metabolic regulation[32]. When a mRNA binds to an enzyme, there is a repression in the translation of the RNA and at the same time, disengagement of the enzyme from its metabolic pathway[33]. LncRNA binding to a metabolic enzyme is an additional dimension to the protein-RNA interaction, where the lncRNA functions to alter the activity of the

enzyme through, as described in these recent cases, changing its interactome[34,35]. Here we show that ADIPINT binds to PC regulating its interaction partners, at least within the mitochondrial fraction of the fat cell and resulting in an increased abundance within the mitochondria and enhanced activity of the enzyme in this compartment. We propose the following role of ADIPINT as a regulator of human fat cell lipid metabolism through PC (Fig. 7). The lncRNA acts as a gate keeper of PC function by controlling the protein interaction partners of PC within the mithochondria. This, in turn, impacts on fat cell lipid and energy metabolism. A critical regulatory step of these pathways is the conversion of pyruvate to oxaloacetate. We presently study white human fat cells so we do not know if ADIPINT is expressed and important for brown or beige human fat cells.

Enzymes form assemblies with other sequential enzymes within a metabolic pathway termed metabolons[26]. These metabolons allow substrate channelling, increasing the flux through the pathway and also increasing the reaction rate for the particular enzyme[27]. We found the interaction of PC with other metabolic enzymes to be disturbed upon ADIPINT knockdown, which may explain why PC activity was reduced even when normalized to the amount of PC. In addition to the metabolic enzymes, metabolons are comprised of additional chaperone proteins such as Hsp70/Hsp90[36], these proteins stabilize the metabolic complex and we found both to be disassociated with PC after ADIPINT knockdown (Supplementary Table 12). As well as additional structual proteins, RNA itself has been shown to act as a scaffold for metabolic enzymes and able to organize metabolite production[37,38]. Unfortunately, the specific interactome of PC has yet to be described in detail and it will require further study to identify the important interacting partners necessary to regulate its localization and reaction rate. It does appear however that ADIPINT plays a role in governing the PC interactome and that this could lead to the changes in PC activity and localization we observed. We found in the prescence of ADIPINT, PC to be interacting with PCK1, the rate limiting enzyme within glyceroneogenesis[28], a process important for fatty-acid re-esterification and fat cell function. As, PC is present in many cell types and tissues, it will be interesting to understand if the adipocyte-specific RNA ADIPINT, is able to establish an adipocyte specific interactome for PC, linking PC to a particular function in WAT.

PC is belived to have its major functions in the mitochondria[30]. Our western blot studies showed two molecular bands of PC, a slightly larger band in the mitochondrial and a slightly smaller band in the cytosolic fraction. Our study found ADIPINT to have stronger effects on the PC interactome in the mitochondria. It is therefore likely that the regulatory role of ADIPINT on PC is most important in this subcellular compartment. PC was previously detected in the cytoplasm in rat adipose tissue[39], however the possible role of PC in the cytosol of adipocytes merits a study of its own.

Our further development of methods to study RNA-protein interactions (TROOPS) greatly facilitated the observation that ADIPINT and PC interact. Methods have previously been developed to investigate the binding of lncRNA to protein[21,22] *in vivo*, though large numbers of cells per replicate are required. By first isolating the RNA-bound proteome before performing targeted pulldown we have reduced the number of cells required to establish the interacting proteins of a given RNA. This modification may be useful in other stem cell or primary cell systems where large quantities of cells are not easily attainable. Previously, PC was only detected as an RNA binding protein when using OOPS[23] or orthogonal approaches[40] in one of the five cell lines examined (endothelial), indicating its interaction with RNA may be cell-type specific. Importantly, we could validate the ability of TROOPS to demonstrate physical interaction between PC and ADIPINT with several independent methods (gel filtration and immunoprecipitation).

PC is a multifaceted regulator of fat cell lipid metabolism[25,28,41,42]. It stimulates triglyceride synthesis and fatty acid re-esterification by increasing de novo fatty acid synthesis and glyceroneogenesis. PC also serves an anaplerotic role in the citric acid cycle[43] by replenishing it with oxaloacetate, generating ATP necessary for lipolysis. This dual PC action (stimulation of lipolysis as well as triglyceride synthesis) places it at a unique position as a potential regulator of fat cell lipid turnover and fat cell size. We previously showed that the WAT lipid turnover is involved in the control of fat mass[4,5] and is linked to dyslipidemia and insulin resistance[44,45]. Furthermore, large fat cells have higher lipolysis and lipid synthesis than small fat cells from the same human WAT specimen[46,47]. Herein we show that ADIPINT regulates both synthesis and breakdown of fat cell lipids *in vitro*. *In vivo* we demonstrate a relationship between ADIPINT expression in WAT and fat cell size, fat mass, insulin sensitivity and circulating lipids. This together suggest a physiological role of ADIPINT in regulating WAT lipid turnover. The influence of ADIPINT expression on hormonal/metabolic parameters is

probably secondary to its influence on fat cell size because the volume of fat cells by itself has a strong impact on fat cell function and clinical parameters[48,49].

Although the contribution of PC to triglyceride homeostasis *in vivo* has not been extensively studied, existing evidence supports an important role. For example, glyceroneogenesis is greatly enhanced following hyperglycemia[50], which occurs after meal ingestion and in diabetic conditions. It is also enhanced *in vivo* in WAT after peroxisome proliferator receptor gamma activation with glitazones[51], with the reduction in plasma fatty acids proposed to be the result of increased re-esterification[52]. Furthermore, knockdown of PC in adipose tissue and liver in rat resulted in reductions in adiposity and improved insulin sensitivity through decreases in lipid re-esterification[53]. PC is also involved in glucose-induced insulin secretion in pancreatic β-cells and gluconeogenesis in the liver[43], and its deficiency can lead to lactic acidosis[54]. Thereby ADIPINT (exclusively expressed in fat cells) could offer a unique way to alter adipocyte PC activity without affecting non-adipose tissues. Obesity influences PC activity and ADIPINT expression in a similar direction and both measures are strongly inter-related. Bearing in mind the strong correlation between a decrease in ADIPINT expression and a decrease in fat mass/fat cell size over time as well as the link to insulin resistance, ADIPINT-PC interactions could have an important clinical role and constitue a pharmacological target for metabolic diseases.

In short, ADIPINT is a novel adipocyte specific polynucleotide that regulates lipid and energy metabolism in part through regulating the mitochondrial interactome of PC and in turn, the activity of the enzyme. The exact molecular mechanism leading ADIPINT to alter PC enzymatic activity remains to be defined. Further studies are needed to establish the consequence of the RNA-protein interaction and suitability as a therapeutic target.

Words (3851/5000)

References

1. Morigny, P., Boucher, J., Arner, P. & Langin, D. Lipid and glucose metabolism in white adipocytes: pathways, dysfunction and therapeutics. *Nat. Rev. Endocrinol.* **0123456789**, (2021).
2. Smith, U. & Kahn, B. B. Adipose tissue regulates insulin sensitivity: role of adipogenesis, de novo lipogenesis and novel lipids. *J. Intern. Med.* **280**, 465–475 (2016).
3. Guilherme, A., Virbasius, J. V, Puri, V. & Czech, M. P. Adipocyte dysfunctions linking obesity to

insulin resistance and type 2 diabetes. *Nat. Rev. Mol. Cell Biol.* **9**, 367–77 (2008).

4. Arner, P. *et al.* Dynamics of human adipose lipid turnover in health and metabolic disease. *Nature* **478**, 110–113 (2011).

5. Arner, P. *et al.* Adipose lipid turnover and long-term changes in body weight. *Nat. Med.* **25**, 1385–1389 (2019).

6. Gao, H. *et al.* Long Non-Coding RNAs Associated with Metabolic Traits in Human White Adipose Tissue. *EBioMedicine* **30**, 248–260 (2018).

7. Hon, C.-C. *et al.* An atlas of human long non-coding RNAs with accurate 5′ ends. *Nature* **543**, (2017).

8. Ransohoff, J. D., Wei, Y. & Khavari, P. A. The functions and unique features of long intergenic non-coding RNA. *Nat. Rev. Mol. Cell Biol.* **19**, 143–157 (2017).

9. Gao, H. *et al.* Long Non-Coding RNAs Associated with Metabolic Traits in Human White Adipose Tissue. *EBioMedicine* **30**, 248–260 (2018).

10. Zhang, X. *et al.* Interrogation of nonconserved human adipose lincRNAs identifies a regulatory role of *linc-ADAL* in adipocyte metabolism. *Sci. Transl. Med.* **10**, eaar5987 (2018).

11. Dallner, O. S. *et al.* Dysregulation of a long noncoding RNA reduces leptin leading to a leptin-responsive form of obesity. *Nat. Med.* **25**, 507–516 (2019).

12. Lin, A. *et al.* The LINK-A lncRNA interacts with PtdIns(3,4,5)P3 to hyperactivate AKT and confer resistance to AKT inhibitors. *Nat. Cell Biol.* **19**, 238–251 (2017).

13. Wang, P. *et al.* The STAT3-binding long noncoding RNA lnc-DC controls human dendritic cell differentiation. *Science (80-.).* **344**, 310–313 (2014).

14. Tran, K. Van *et al.* Human thermogenic adipocyte regulation by the long noncoding RNA LINC00473. *Nat. Metab.* **2**, 397–412 (2020).

15. Salans, L. B., Knittle, J. L. & Hirsch, J. The role of adipose cell size and adipose tissue insulin sensitivity in the carbohydrate intolerance of human obesity. *J. Clin. Invest.* **47**, 153–165 (1968).

16. Hoffstedt, J. *et al.* Long-term protective changes in adipose tissue after gastric bypass. *Diabetes Care* **40**, 77–84 (2017).

17. Kerr, A. G., Andersson, D. P., Ryden, M., Arner, P. & Dahlman, I. Long-term changes in adipose tissue gene expression following bariatric surgery. *J. Intern. Med.* **288**, 219–233 (2020).

18. Ehrlund, A. *et al.* Transcriptional dynamics during human adipogenesis and its link to adipose morphology and distribution. *Diabetes* **66**, 218–230 (2017).

19. Lee, J. H. *et al.* The role of adipose tissue mitochondria: Regulation of mitochondrial function for the treatment of metabolic diseases. *Int. J. Mol. Sci.* **20**, (2019).

20. Mackall, J. C. & Daniel Lane, M. Role of pyruvate carboxylase in fatty acid synthesis: Alterations during preadipocyte differentiation. *Biochem. Biophys. Res. Commun.* **79**, 720–725 (1977).

21. Chu, C. *et al.* Systematic discovery of Xist RNA binding proteins. *Cell* **161**, 404–16 (2015).

22. Simon, M. D. *et al.* The genomic binding sites of a noncoding RNA. *Proc. Natl. Acad. Sci. U. S. A.* **108**, 20497–502 (2011).

23. Queiroz, R. M. L. *et al.* Comprehensive identification of RNA–protein interactions in any organism using orthogonal organic phase separation (OOPS). *Nat. Biotechnol.* **37**, 169–178 (2019).

24. Chang, C. H. *et al.* Posttranscriptional control of T cell effector function by aerobic glycolysis. *Cell* **153**, 1239 (2013).

25. Jitrapakdee, S. *et al.* Structure, mechanism and regulation of pyruvate carboxylase. *Biochem. J.* **413**, 369–387 (2008).

26. Srere, P. A. Complexes of sequential metabolic enzymes. *Annu. Rev. Biochem.* **56**, 89–124 (1987).

27. Sweetlove, L. J. & Fernie, A. R. The role of dynamic enzyme assemblies and substrate channelling in metabolic regulation. *Nat. Commun.* **9**, (2018).

28. Reshef, L. *et al.* Glyceroneogenesis and the triglyceride/fatty acid cycle. *Journal of Biological Chemistry* **278**, 30413–30416 (2003).

29. Si, Y., Shi, H. & Lee, K. Impact of perturbed pyruvate metabolism on adipocyte triglyceride accumulation. *Metab. Eng.* **11**, 382–390 (2009).

30. Utter, M. F. & Scrutton, M. C. Pyruvate Carboxylase. *Curr. Top. Cell. Regul.* **1**, 253–296 (1969).

31. Yount, E. A. & Harris, R. Studies on the inhibition of gluconeogenesis by oxalate. **633**, 122–133 (1980).

32. Castello, A., Hentze, M. W. & Preiss, T. Metabolic Enzymes Enjoying New Partnerships as RNA-Binding Proteins. *Trends Endocrinol. Metab.* **26**, 746–757 (2015).

33. Hentze, M. W., Castello, A., Schwarzl, T. & Preiss, T. A brave new world of RNA-binding proteins. *Nat. Rev. Mol. Cell Biol.* **19**, 327–341 (2018).

34. Sang, L. *et al.* Mitochondrial long non-coding RNA GAS5 tunes TCA metabolism in response to nutrient stress. *Nat. Metab.* **3**, 90–106 (2021).

35. Wang, C. *et al.* Interactome analysis reveals that lncRNA HULC promotes aerobic glycolysis through LDHA and PKM2. *Nat. Commun.* **11**, (2020).

36. French, J. B. *et al.* Hsp70/Hsp90 chaperone machinery is involved in the assembly of the purinosome. *Proc. Natl. Acad. Sci. U. S. A.* **110**, 2528–2533 (2013).

37. Sachdeva, G., Garg, A., Godding, D., Way, J. C. & Silver, P. A. In vivo co-localization of enzymes on RNA scaffolds increases metabolic production in a geometrically dependent manner. *Nucleic Acids Res.* **42**, 9493–9503 (2014).

38. Delebecque, C. J., Lindner, A. B., Silver, P. A. & & Aldaye, F. A. Organization of Intracellular Reactions with Rationally Designed RNA Assemblies. *Science (80-.).* 470–474 (2011).

39. Reshef, L., Hanson, R. W. & Ballard, F. J. Glyceride-glycerol synthesis from pyruvate. Adaptive changes in phosphoenolpyruvate carboxykinase and pyruvate carboxylase in adipose tissue and liver. *J. Biol. Chem.* **244**, 1994–2001 (1969).

40. Trendel, J. *et al.* The Human RNA-Binding Proteome and Its Dynamics during Translational Arrest. *Cell* **176**, 391-403.e19 (2019).

41. Proença, A. R. G. *et al.* New concepts in white adipose tissue physiology. *Brazilian Journal of Medical and Biological Research* **47**, 192–205 (2014).

42. Kopecky, J. *et al.* Modulation of Lipid Metabolism by Energy Status of Adipocytes. *Ann. N. Y. Acad. Sci.* **967**, 88–101 (2006).

43. Jitrapakdee, S., Vidal-Puig, A. & Wallace, J. C. Anaplerotic roles of pyruvate carboxylase in mammalian tissues. *Cell. Mol. Life Sci.* **63**, 843–854 (2006).

44. Frayn, K., Bernard, S., Spalding, K. & Arner, P. Adipocyte triglyceride turnover is independently associated with atherogenic dyslipidemia. *J. Am. Heart Assoc.* **1**, (2012).

45. Spalding, K. L. *et al.* Impact of fat mass and distribution on lipid turnover in human adipose tissue. *Nat. Commun.* **8**, 1–9 (2017).

46. Smith, U. Effect of cell size on lipid synthesis by human adipose tissue in vitro. *J. Lipid Res.* **12**, 65–70 (1971).

47. Laurencikiene, J. *et al.* Regulation of Lipolysis in Small and Large Fat Cells of the Same Subject. *J.*

Clin. Endocrinol. Metab. **96**, E2045–E2049 (2011).

48. Laforest, S., Labrecque, J., Michaud, A., Cianflone, K. & Tchernof, A. Adipocyte size as a determinant of metabolic disease and adipose tissue dysfunction. *Crit. Rev. Clin. Lab. Sci.* **52**, 301–313 (2015).

49. Stenkula, K. G. & Erlanson-Albertsson, C. Adipose cell size: Importance in health and disease. *Am. J. Physiol. - Regul. Integr. Comp. Physiol.* **315**, R284–R295 (2018).

50. Rotondo, F. *et al.* Glycerol is synthesized and secreted by adipocytes to dispose of excess glucose, via glycerogenesis and increased acyl-glycerol turnover. *Sci. Rep.* **7**, 1–14 (2017).

51. Cadoudal, T. *et al.* Acute and selective regulation of glyceroneogenesis and cytosolic phosphoenolpyruvate carboxykinase in adipose tissue by thiazolidinediones in type 2 diabetes. *Diabetologia* **50**, 666–675 (2007).

52. Leroyer, S. N. *et al.* Rosiglitazone controls fatty acid cycling in human adipose tissue by means of glyceroneogenesis and glycerol phosphorylation. *J. Biol. Chem.* **281**, 13141–13149 (2006).

53. Kumashiro, N. *et al.* Targeting pyruvate carboxylase reduces gluconeogenesis and adiposity and improves insulin resistance. *Diabetes* **62**, 2183–2194 (2013).

54. García-Cazorla, A. *et al.* Pyruvate carboxylase deficiency: Metabolic characteristics and new neurological aspects. *Ann. Neurol.* **59**, 121–127 (2006).

55. Andersson, D. P., Arner, E., Hogling, D. E., Rydén, M. & Arner, P. Abdominal subcutaneous adipose tissue cellularity in men and women. *Int. J. Obes.* **41**, 1564–1569 (2017).

56. Gao, H. *et al.* CD36 Is a Marker of Human Adipocyte Progenitors with Pronounced Adipogenic and Triglyceride Accumulation Potential. *Stem Cells* **35**, 1799–1814 (2017).

57. Hellmér, J., Arner, P. & Lundin, A. Automatic luminometric kinetic assay of glycerol for lipolysis studies. *Anal. Biochem.* **177**, 132–137 (1989).

58. Barquissau, V. *et al.* White-to-brite conversion in human adipocytes promotes metabolic reprogramming towards fatty acid anabolic and catabolic pathways. *Mol. Metab.* **5**, 352–365 (2016).

59. Ruan, X., Li, P. & Cao, H. Identification of transcriptional regulators that bind to long noncoding RNAs by RNA pull-down and RNA immunoprecipitation. *Methods Mol. Biol.* **1783**, 185–191 (2018).

60. Wessel, D. & Flügge, U. I. A method for the quantitative recovery of protein in dilute solution in the presence of detergents and lipids. *Anal. Biochem.* **138**, 141–143 (1984).

61. Smyth, G. K. Linear Models and Empirical Bayes Methods for Assessing Differential Expression in Microarray Experiments. *Stat. Appl. Genet. Mol. Biol.* **3**, 1–25 (2004).

Figures

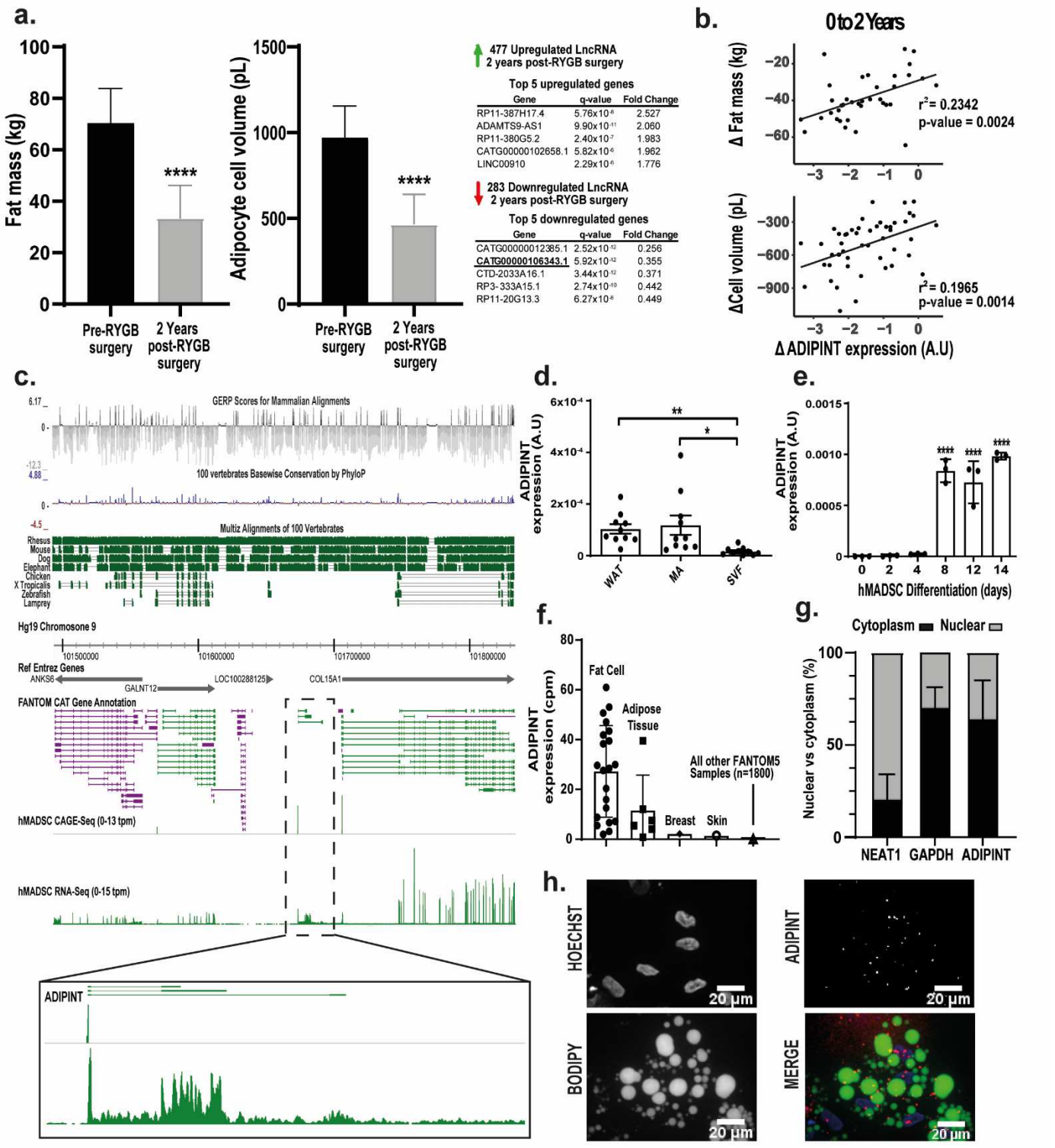
a.
Fat mass (kg)
Pre-RYGB surgery
2 Years post-RYGB surgery
****
Adipocyte cell volume (pL)
477 Upregulated LncRNA
2 years post-RYGB surgery
Top 5 upregulated genes
Gene q-value Fold Change
RP11-387H17.4 5.76x10-8 2.527
ADAMTS9-AS1 9.90x10-11 2.060
RP11-380G5.2 2.40x10-7 1.983
CATG00000102658.1 5.82x10-6 1.962
LINC00910 2.29x10-6 1.776
283 Downregulated LncRNA
2 years post-RYGB surgery
Top 5 downregulated genes
Gene q-value Fold Change
CATG00000012385.1 2.52x10-12 0.256
CATG00000106343.1 5.92x10-12 0.355
CTD-2033A16.1 3.44x10-12 0.371
RP3-333A15.1 2.74x10-10 0.442
RP11-20G13.3 6.27x10-8 0.449
b.
0 to 2 Years
Δ Fat mass (kg)
r2= 0.2342
p-value = 0.0024
ΔCell volume (pL)
r2= 0.1965
p-value = 0.0014
Δ ADIPINT expression (A.U)
c.
GERP Scores for Mammalian Alignments
100 vertebrates Basewise Conservation by PhyloP
Multiz Alignments of 100 Vertebrates
Rhesus
Mouse
Dog
Elephant
Chicken
X Tropicalis
Zebrafish
Lamprey
Hg19 Chromosome 9
Ref Entrez Genes
ANKS6
GALNT12
LOC100288125
COL15A1
FANTOM CAT Gene Annotation
hMADSC CAGE-Seq (0-13 tpm)
hMADSC RNA-Seq (0-15 tpm)
ADIPINT
d.
ADIPINT expression (A.U)
WAT
MA
SVF
e.
ADIPINT expression (A.U)
hMADSC Differentiation (days)
f.
ADIPINT expression (cpm)
Fat Cell
Adipose Tissue
Breast
Skin
All other FANTOM5 Samples (n=1800)
g.
Cytoplasm
Nuclear
Nuclear vs cytoplasm (%)
NEAT1
GAPDH
ADIPINT
h.
HOECHST
ADIPINT
BODIPY
MERGE
20 µm

Fig. 1: The adipocyte-specific lncRNA ADIPINT (CATG00000106343.1) is linked to changes in fat mass and fat cell volume

a Identification of differentially-expressed lncRNAs two years post- Roux-en-Y gastric bypass (RYGB) surgery compared to pre-RYGB. Fifty WAT samples were examined at baseline and compared with 49 from patients returning after two years. The changes in fat mass and fat cell volume were compared by paired t-test and the number of altered lncRNAs at two years compared to baseline is shown to the right. The five lncRNA with the greatest increase or decrease in fold change at two years are listed, including ADIPINT (CATG00000106343.1). **b** Correlation of the change in ADIPINT expression versus the change in total fat mass or adipocyte cell volume from zero to two years post-RYGB. Each data point represents an individual patient (data for gene expression and fat cell size were available from 49 women; gene expression and fat mass were available from 37). Linear regression was used to assess significance. **c** Genomic position of ADIPINT on chromosome 9 (annotated by the FANTOM-CAT gene model) is indicated and the expression detected by RNA-Seq and CAGE-Seq in human adipose-derived stem cells (hADSC) at day 14 of differentiation is shown. The conservation of the ADIPINT genomic region in mammalian and non-mammalian species is displayed above. **d** qRT-PCR analysis of ADIPINT expression in fractionated mature adipocytes (MA) and stroma-vascular fraction cells (SVF) from human WAT. **e** qRT-PCR analysis of ADIPINT during *in vitro* hADSC differentiation into adipocytes. Each data point represents an individual experiment. One-way ANOVA with Dunnett's post-hoc test was used to assess significance compared to day 0 of differentiation and one-way ANOVA with Holm-Sidak's post-hoc test was used to assess significance between WAT fractionation samples. **f** CAGE-Seq ADIPINT expression in all FANTOM5 samples. Samples with detected expression (counts per million (cpm)) are plotted; no expression was detected in any other cell or tissue types in the FANTOM5 samples not annotated. **g** Fractionation of hADSC cells at day 13 of differentiation followed by qRT-PCR of ADIPINT. NEAT1 and GAPDH were used to validate the nuclear and cytoplasmic fractions, respectively. Five independent experiments are shown for NEAT1 and GAPDH and three for ADIPINT. **h** RNA-FISH for ADIPINT in hADSC at day 13 of differentiation, staining for nuclei (HOECHST-Blue) and lipid (BODIPY-Green) alongside fluorescent probes targeting ADIPINT (Red). The experiment was performed three times with similar results. Scale bar, 20 μm. Error bars are SD for $n < 6$ and SEM for $n \geq 6$. * < 0.05, **** < 0.0001.

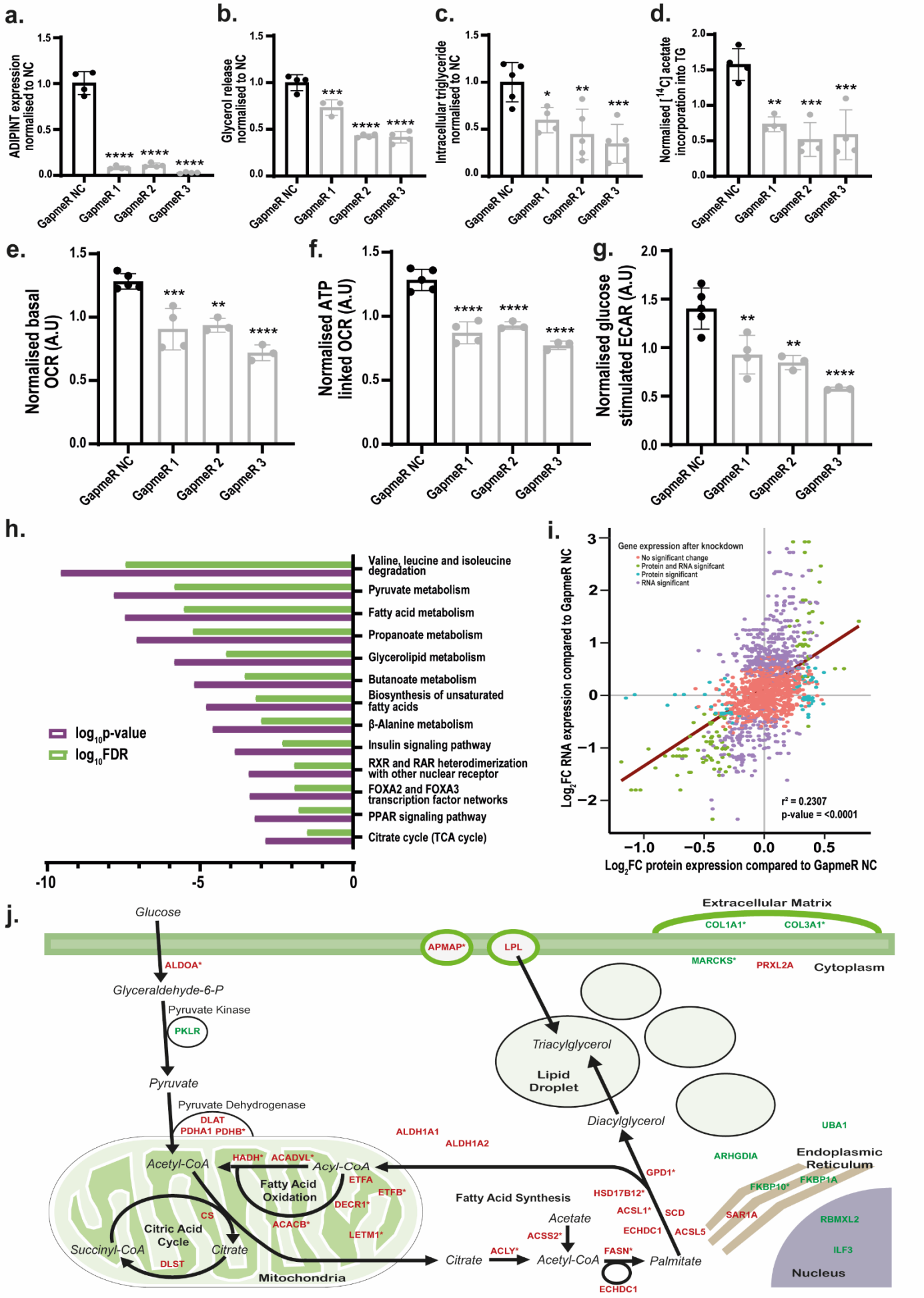
a.
ADIPINT expression normalised to NC
b.
Glycerol release normalised to NC
c.
Intracellular triglyceride normalised to NC
d.
Normalised [14C] acetate incorporation into TG
GapmeR NC
GapmeR 1
GapmeR 2
GapmeR 3
e.
Normalised basal OCR (A.U)
f.
Normalised ATP linked OCR (A.U)
g.
Normalised glucose stimulated ECAR (A.U)
h.
Valine, leucine and isoleucine degradation
Pyruvate metabolism
Fatty acid metabolism
Propanoate metabolism
Glycerolipid metabolism
Butanoate metabolism
Biosynthesis of unsaturated fatty acids
β-Alanine metabolism
Insulin signaling pathway
RXR and RAR heterodimerization with other nuclear receptor
FOXA2 and FOXA3 transcription factor networks
PPAR signaling pathway
Citrate cycle (TCA cycle)
log10p-value
log10FDR
i.
Gene expression after knockdown
No significant change
Protein and RNA signifcant
Protein significant
RNA significant
Log2FC RNA expression compared to GapmeR NC
Log2FC protein expression compared to GapmeR NC
r² = 0.2307
p-value = <0.0001
j.
Glucose
ALDOA*
Glyceraldehyde-6-P
Pyruvate Kinase
PKLR
Pyruvate
Pyruvate Dehydrogenase
DLAT
PDHA1 PDHB*
Acetyl-CoA
HADH*
ACADVL*
Acyl-CoA
ETFA
ETFB*
Fatty Acid Oxidation
DECR1*
ACACB*
LETM1*
CS
Citric Acid Cycle
Succinyl-CoA
Citrate
DLST
Mitochondria
Citrate
ACLY*
Acetyl-CoA
Acetate
ACSS2*
Fatty Acid Synthesis
FASN*
ECHDC1
Palmitate
ALDH1A1
ALDH1A2
Diacylglycerol
Triacylglycerol
Lipid Droplet
APMAP*
LPL
Extracellular Matrix
COL1A1*
COL3A1*
MARCKS*
PRXL2A
Cytoplasm
GPD1*
HSD17B12*
ACSL1*
SCD
ECHDC1
ACSL5
UBA1
ARHGDIA
Endoplasmic Reticulum
FKBP10*
FKBP1A
SAR1A
RBMXL2
ILF3
Nucleus

Fig. 2: Knockdown of ADIPINT perturbs lipid metabolism and bioenergetics

a ADIPINT expression **b** glycerol release (measure of basal lipolysis) **c** intracellular triglyceride content and **d** insulin stimulated [^{14}C] acetate incorporation into intracellular lipid (measure of lipid synthesis) in hADSC transfected with three ADIPINT targeting GapmeRs (1-3) or non-targeting control GapmeR (NC). Each data point represents an individual experiment. **a-c** Mean normalized to GapmeR NC and **d** mean normalized to GapmeR NC (-insulin). **e** Basal and **f** ATP linked oxygen consumption rate (OCR) and **g** Glucose-stimulated extracellular acidification rate (ECAR) in hADSC transfected with three ADIPINT targeting GapmeRs (1-3) or non-targeting control GapmeR (NC). ATP linked OCR was determined after oligomycin administration. ECR determined after glucose treatment. Each experiment was normalized to the average OCR/ECR of that experiment. **a-g** One-way ANOVA with Dunnett's post-hoc test was used to assess significance between GapmeR NC and GapmeRs 1-3. **h** The $\log_2$ fold change in RNA plotted against the $\log_2$ fold change in protein for each gene detected at the RNA and protein level, after transfection with GapmeRs as described above. The median fold change across the three ADIPINT-targeting GapmeRs (1-3) compared to GapmeR NC is plotted and the median false discovery rate (FDR) was used to determine if an RNA or protein is significantly altered. All genes are plotted except TF which was significantly altered at the RNA ($\log_2$FC = 6.6) but not protein level. Linear regression was used to assess significance between global changes in RNA and protein. **i** Pathways enriched by genes downregulated after ADIPINT knockdown by each GapmeR independently, compared to GapmeR NC. **j** A schematic diagram of all 38 proteins significantly altered independently by all three GapmeRs targeting ADIPINT. Proteins are displayed based on the associated metabolic pathway and localization according to www.genecards.org. Proteins downregulated following ADIPINT knockdown are in red font and upregulated are in green font. Proteins marked with * were not significantly regulated at the RNA level. If no metabolic pathway was listed for the given protein, then the protein was placed on the diagram based on the given subcellular localization. Metabolites were not measured. Error bars are SD. * < 0.05, ** < 0.01, *** < 0.001, **** < 0.0001.

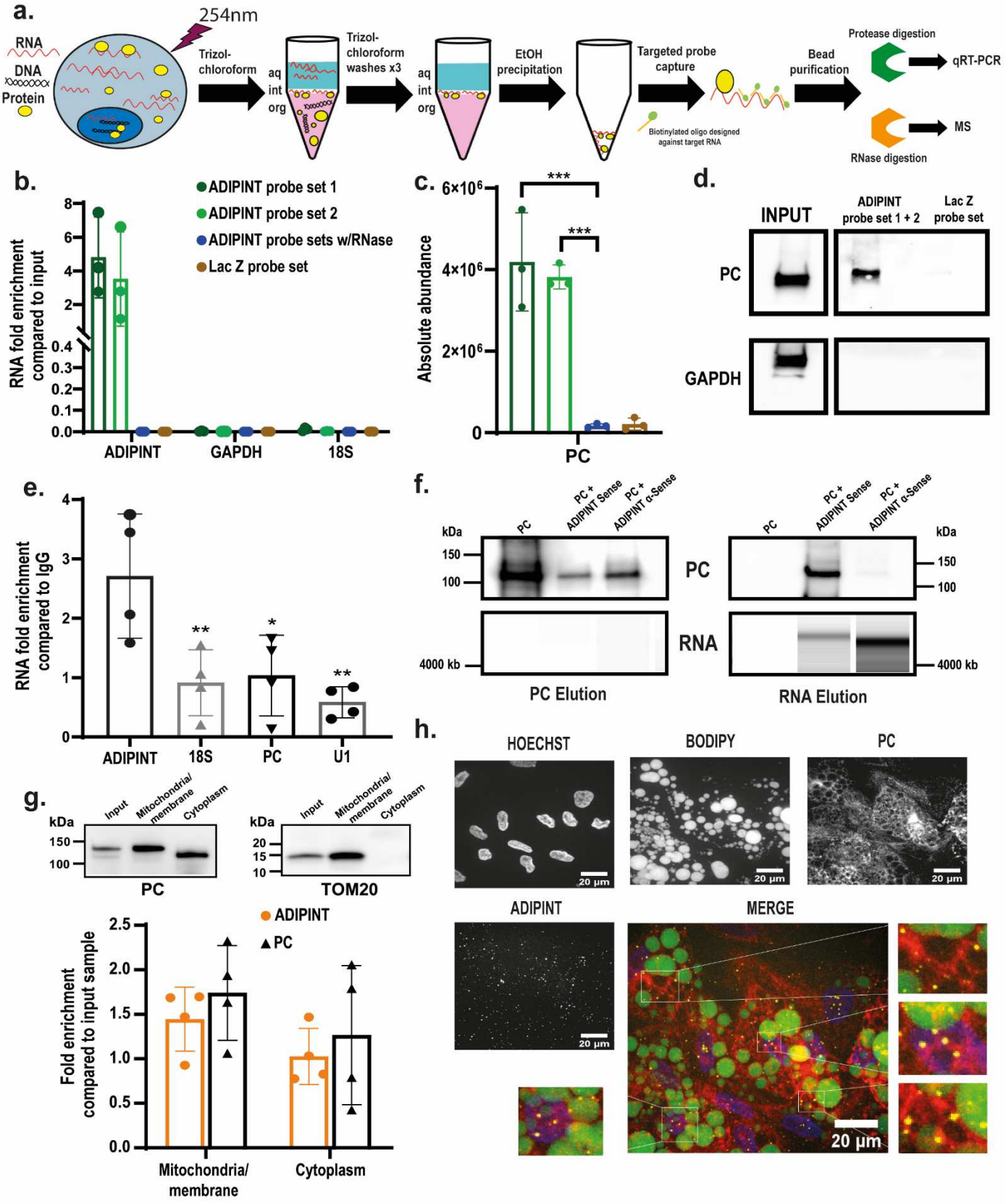
a.
254nm
RNA
DNA
Protein
Trizol-chloroform
aq
int
org
Trizol-chloroform washes x3
EtOH precipitation
Targeted probe capture
Biotinylated oligo designed against target RNA
Bead purification
Protease digestion
qRT-PCR
MS
RNase digestion
b.
ADIPINT probe set 1
ADIPINT probe set 2
ADIPINT probe sets w/RNase
Lac Z probe set
RNA fold enrichment compared to input
ADIPINT
GAPDH
18S
c.
Absolute abundance
PC
d.
INPUT
ADIPINT probe set 1 + 2
Lac Z probe set
PC
GAPDH
e.
RNA fold enrichment compared to IgG
ADIPINT
18S
PC
U1
f.
PC
PC + ADIPINT Sense
PC + ADIPINT α-Sense
kDa
PC Elution
RNA Elution
RNA
4000 kb
g.
Input
Mitochondria/ membrane
Cytoplasm
PC
TOM20
Fold enrichment compared to input sample
Mitochondria/ membrane
Cytoplasm
h.
HOECHST
BODIPY
PC
ADIPINT
MERGE
20 µm

485

486

Fig. 3: **Targeted RNA-protein identification using orthogonal organic phase separation (TROOPS) identifies pyruvate carboxylase as an interacting partner of ADIPINT**

a Graphical representation of TROOPS methodology. **b** qRT-PCR analysis of ADIPINT, 18S and GAPDH expression in TROOPS pulldown samples using short oligos targeting ADIPINT or Lac Z (RNA not expressed in human cells). Data is presented as fold increase compared to an input sample collected before pulldown. No ADIPINT expression was detected in ADIPINT targeting probes with RNase or Lac Z targeting probe sets. **c** Absolute abundance values obtained from mass-spectrometry for pyruvate carboxylase in each probe set targeting ADIPINT or Lac Z. Statistical comparisons were made between each probe set and ADIPINT probe sets 1 and 2 in the presence of RNase using one-way ANOVA with Dunnett's post-hoc test. **d** Western blot analysis of PC and GAPDH after TROOPS pulldown using odd and even probes targeting ADIPINT or Lac Z probes. **e** RNA immunoprecipitation (RIP) pulldown using PC or IgG targeting antibody followed by qRT-PCR for ADIPINT, 18S, PC and U1. The fold increase in PC pulldown samples compared to IgG is plotted and statistical comparisons are made comparing ADIPINT with 18S, PC and U1 using one-way ANOVA with Dunnett's post-hoc test. **f** Western blot analysis (top panel) for PC and RNA analysis (bottom panel) using a BioAnalyzer after column filtration of PC alone or in the prescence of ADIPINT or ADIPINT anti-sense. RNA and PC were loaded at a molar ratio of 0:25:1. The fractions that PC and ADIPINT/ADIPINT anti-sense elute at were collected (labelled PC elution and RNA elution) and analysed. **g** Cellular fractionation of hADSC into mitochondrial/membrane and cytoplasmic compartments by ultracentrifugation. Above, a representative western blot showing PC and TOM20 staining (mitochondrial marker protein) in each fraction. Below PC and ADIPINT expression in each fraction quantified and expressed as fold increase compared to an input sample taken before separation. Each data point represents an individual experiment;for TROOPS the same experiment was used for RNA and mass-spectrometry analysis. **h** RNA-FISH and immunofluorescence in tandem in hADSC staining nuclei (HOECHST-Blue), lipid (BODIPY-Green), PC (α-PC-Red) and ADIPINT (RNA FISH-Yellow). A representative image is presented for each individual channel and as a merge of all four channels. Zoomed in boxes to the right of the merged image are presented to highlight overlapping PC and ADIPINT fluorescence. Scale bar is 20 μm. Error bars are SD. * < 0.05, ** < 0.01, *** < 0.001, **** < 0.0001.

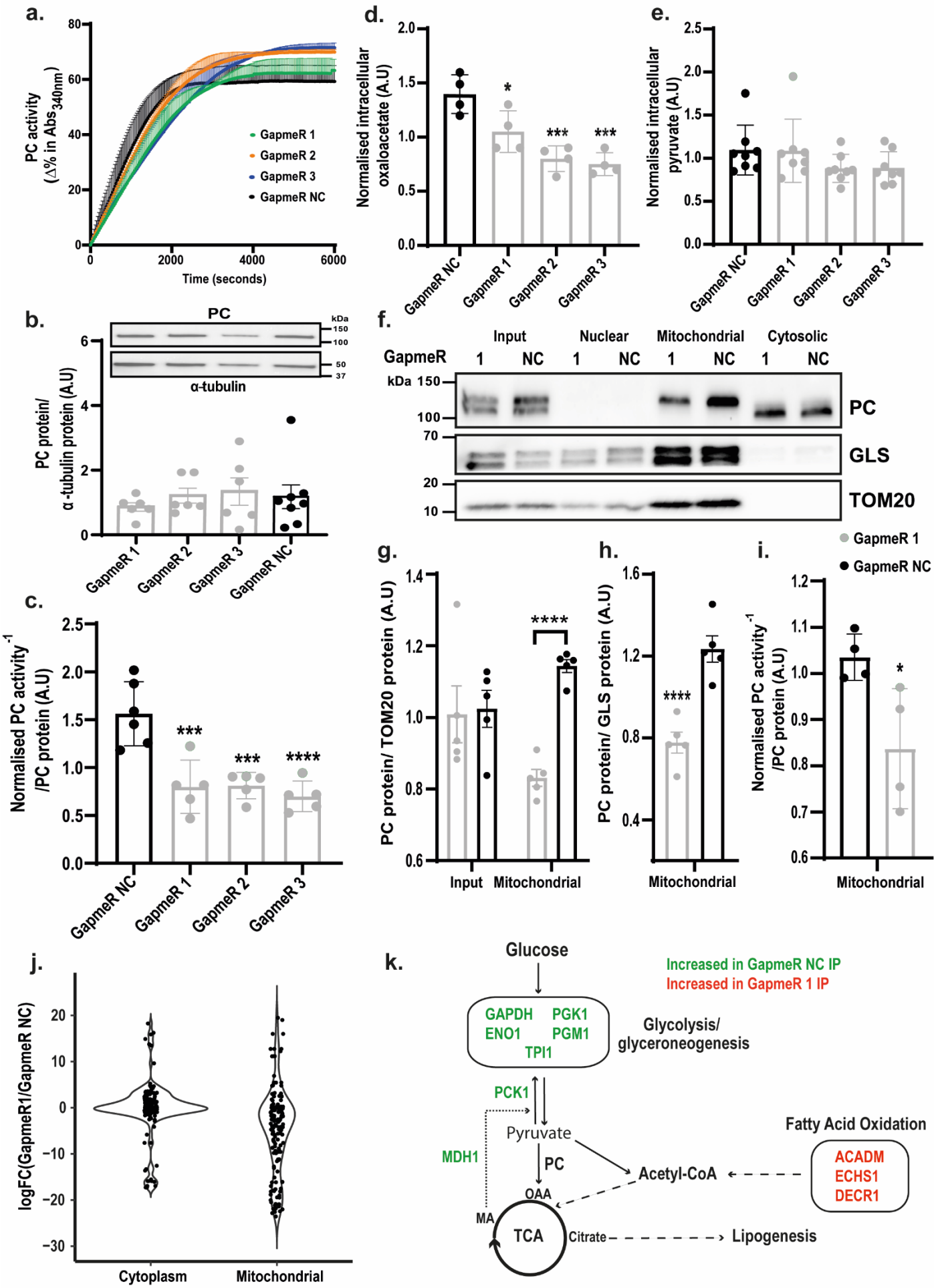
a.
PC activity (Δ% in Abs340nm)
Time (seconds)
GapmeR 1
GapmeR 2
GapmeR 3
GapmeR NC
b.
PC
α-tubulin
kDa
PC protein/ α-tubulin protein (A.U)
c.
Normalised PC activity-1 /PC protein (A.U)
d.
Normalised intracellular oxaloacetate (A.U)
e.
Normalised intracellular pyruvate (A.U)
f.
Input
Nuclear
Mitochondrial
Cytosolic
GapmeR
PC
GLS
TOM20
g.
PC protein/ TOM20 protein (A.U)
h.
PC protein/ GLS protein (A.U)
i.
Normalised PC activity-1 /PC protein (A.U)
j.
logFC(GapmeR1/GapmeR NC)
Cytoplasm
Mitochondrial
k.
Glucose
Increased in GapmeR NC IP
Increased in GapmeR 1 IP
GAPDH
PGK1
ENO1
PGM1
TPI1
Glycolysis/ glyceroneogenesis
PCK1
Pyruvate
MDH1
PC
Acetyl-CoA
Fatty Acid Oxidation
ACADM
ECHS1
DECR1
OAA
MA
TCA
Citrate
Lipogenesis

Fig. 4: ADIPINT knockdown reduces mitochondrial pyruvate carboxylase activity and abundance

a PC activity measured through a change in absorbance of NADH (340 nm) after transfection with GapmeR NC (black) or ADIPINT-targeting GapmeRs 1-3. The lines represent three independent experiments assayed at the same time. No differences in the total amount of substrate metabolized by PC was detected across all experiments. The time to reach 50% completion of the reaction in the displayed experiments was 1654 (GapmeR 1), 1396 (GapmeR 2), 2233 (GapmeR 3) and 808 (GapmeR NC) seconds and was used as a measure of PC activity. **b** Western blot quantification of PC protein and α-tubulin (housekeeping protein) in the same sample PC activity was measured. PC expression is normalized to α-tubulin. One representative western blot for PC and α-tubulin is given above. **c** Normalization of PC activity by PC expression. PC activity and protein were normalized per experiment and each data point represents an individual experiment. **d** Intracellular oxaloacetate and **e** pyruvate levels normalized per experiment after ADIPINT knockdown using GapmeRs 1-3. Target and control GapmeRs were compared by one-way ANOVA with Dunnett's post-hoc test to assess significance. **f** Representative western blot for PC and the mitochondria-localized proteins TOM20 and Glutaminase (GLS) after cellular fractionation into nuclei, mitochondrial and cytoplasmic fractions. **g** Quantification of PC abundance in input and mitochondrial fractions normalized to TOM20 and **h** GLS. **i** PC activity measured in the mitochondrial fraction after ADIPINT knockdown using GapmeR 1. Two-tailed t-test was used to compare significance between GapmeR 1 and Gapmer NC samples in the input and mitochondrial fractions. **j** The distribution of the $\log_2$ fold changes for proteins after PC immunoprecipitation in the mitochondrial and cytoplasmic fractions following ADIPINT knockdown with GapmeR 1. **k** Graphical representation of enzymes involved in the glycolysis/glycernoneogenesis, energy metabolism and fatty acid oxidation pathways altered in PC immunoprecipitation samples following ADIPINT knockdown. Green font indicates proteins that were higher in GapmeR NC samples and red font that were higher in GapmeR 1 samples. Error bars are SD for $n < 6$ and SEM for $n \geq 6$. * < 0.05, ** < 0.01, *** < 0.001, **** < 0.0001.

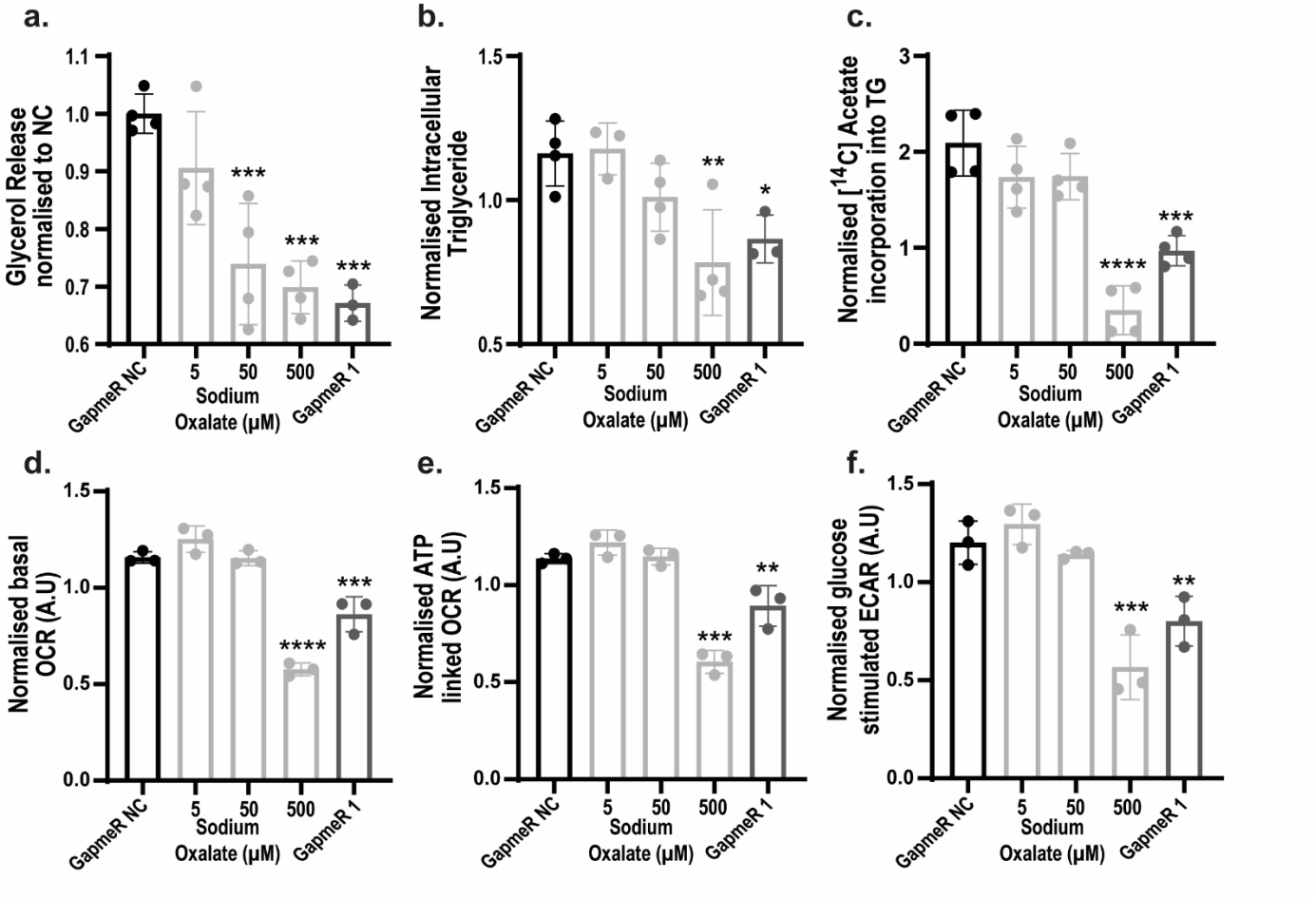
a.
Glycerol Release normalised to NC
1.1
1.0
0.9
0.8
0.7
0.6
***
***
***
GapmeR NC
5
50
500
GapmeR 1
Sodium Oxalate (µM)
b.
Normalised Intracellular Triglyceride
1.5
1.0
0.5
**
*
GapmeR NC
5
50
500
GapmeR 1
Sodium Oxalate (µM)
c.
Normalised [14C] Acetate incorporation into TG
3
2
1
0
****
***
GapmeR NC
5
50
500
GapmeR 1
Sodium Oxalate (µM)
d.
Normalised basal OCR (A.U)
1.5
1.0
0.5
0.0
****
***
GapmeR NC
5
50
500
GapmeR 1
Sodium Oxalate (µM)
e.
Normalised ATP linked OCR (A.U)
1.5
1.0
0.5
0.0
***
**
GapmeR NC
5
50
500
GapmeR 1
Sodium Oxalate (µM)
f.
Normalised glucose stimulated ECAR (A.U)
1.5
1.0
0.5
0.0
***
**
GapmeR NC
5
50
500
GapmeR 1
Sodium Oxalate (µM)

Fig. 5: Pyruvate carboxylase inhibition recapitulates the effects on lipid metabolism and bioenergetics as seen with ADIPINT knockdown

a glycerol release (measure of basal lipolysis) **b** intracellular triglyceride content and **c** insulin-stimulated [^{14}C] acetate incorporation into intracellular lipid (measure of lipid synthesis) in hADSC incubated with varying concentrations of oxalate. **e** Basal and **f** ATP-linked OCR and **g** Glucose-stimulated ECAR in hADSC after oxalate administration. ADIPINT knockdown using GapmeR 1 was used as a positive control for the effects on glycerol release, triglyceride content, lipid synthesis, OCR and ECAR. Each data point represents an individual experiment. One-way ANOVA with Dunnett's post-hoc test assessed significance between GapmeR NC versus GapmeR NC plus oxalate treatment and GapmeR 1. Error bars are SD. * < 0.05, ** < 0.01, *** < 0.001, **** < 0.0001.

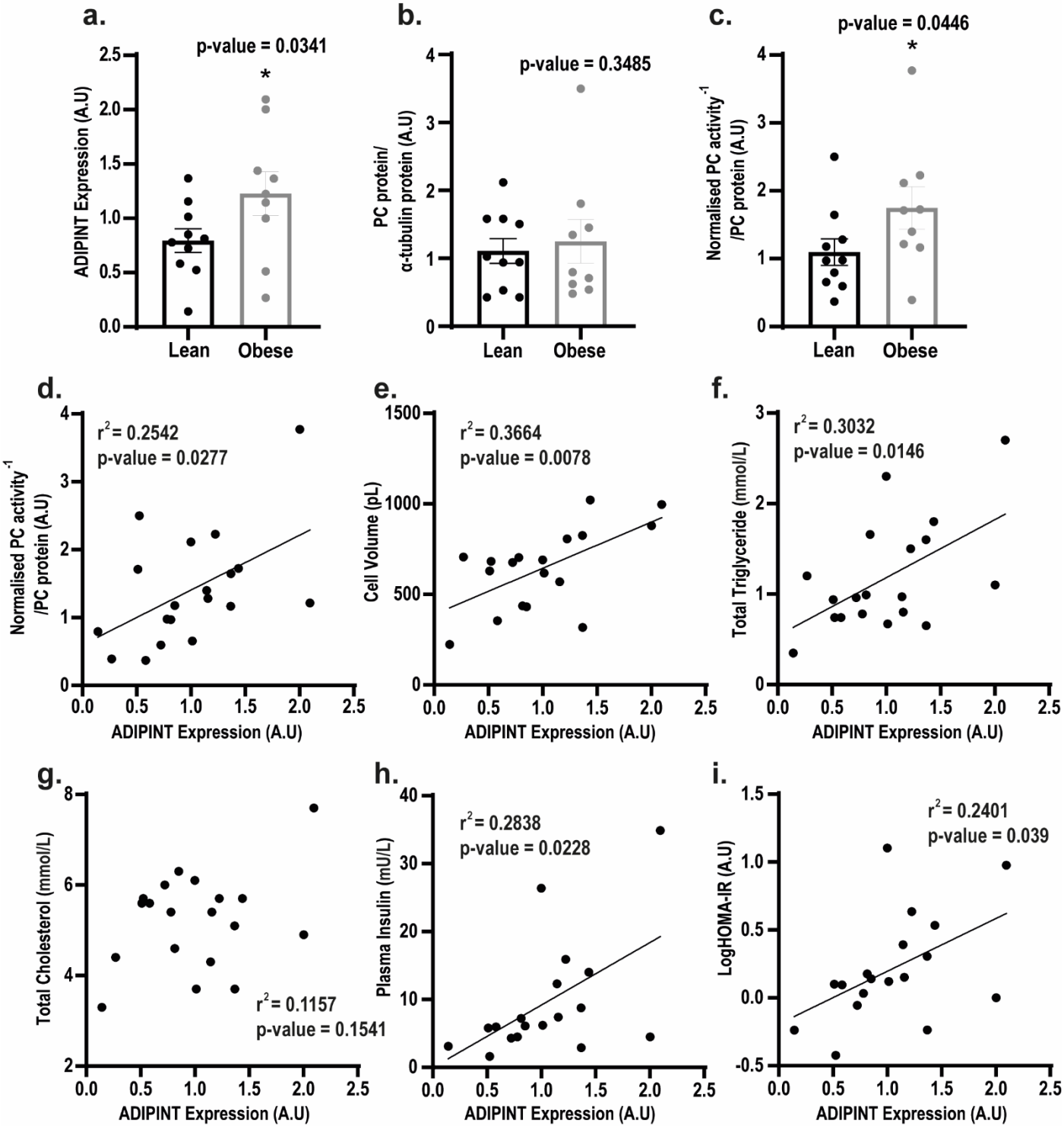
a.
p-value = 0.0341
*
ADIPINT Expression (A.U)
Lean
Obese
b.
p-value = 0.3485
PC protein/
α-tubulin protein (A.U)
Lean
Obese
c.
p-value = 0.0446
*
Normalised PC activity-1
/PC protein (A.U)
Lean
Obese
d.
r2= 0.2542
p-value = 0.0277
Normalised PC activity-1
/PC protein (A.U)
ADIPINT Expression (A.U)
e.
r2= 0.3664
p-value = 0.0078
Cell Volume (pL)
ADIPINT Expression (A.U)
f.
r2= 0.3032
p-value = 0.0146
Total Triglyceride (mmol/L)
ADIPINT Expression (A.U)
g.
r2= 0.1157
p-value = 0.1541
Total Cholesterol (mmol/L)
ADIPINT Expression (A.U)
h.
r2= 0.2838
p-value = 0.0228
Plasma Insulin (mU/L)
ADIPINT Expression (A.U)
i.
r2= 0.2401
p-value = 0.039
LogHOMA-IR (A.U)
ADIPINT Expression (A.U)

Fig. 6: Subcutaneous adipose ADIPINT expression and PC activity are increased in obesity and correlate with each other

Analyses of **a** PC activity and **b** PC and **c** ADIPINT expression in subcutaneous adipose tissue of 9 obese and 10 lean apparently healthy women. A body mass index (BMI) of 30 kg/m^2 was used to distinguish obese and non-obese patients. PC activity was normalized to PC protein expression from the same adipose tissue sample. A one-tailed t-test was used to asses significance between lean and obese. ADIPINT expression was correlated with **d** PC activity, **e** cell volume, **f** plasma triglycerides, **g** total cholesterol, **h** plasma insulin and **i** logHOMA-IR, measured in all lean and obese samples. HOMA is a measure of the level of overall insulin resistance in vivo (fasting insulin times fasting glucose divided by 22.5). Linear regression assessed significance in correlation analyses. Each data point represents an individual patient, error bars represent SEM.

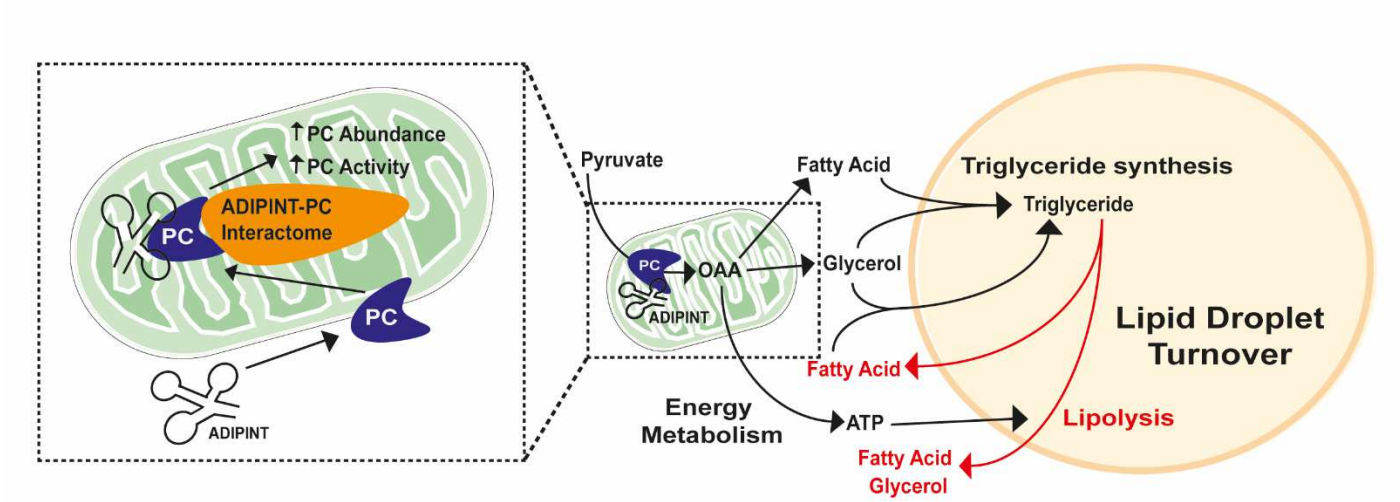

Fig. 7: Current working model for the effect of the ADIPINT-PC interaction on fat cell metabolism

ADIPINT interacts with PC regulating its interactome which results in an increased abundance and activity of PC within the mitochondria. The increase in PC activity leads to the increased production of oxaloacetate (OAA) used for lipid synthesis and breakdown and energy metabolism in the adipocyte.

Methods

Clinical cohort

We included women with obesity who were subjected to Roux-en-y gastric bypass (RYGB) and have been described previously for other type of studies[16,17] (DEOSH, trial registration number NCT01785134). Clinical data extracted from previous publications are presented in Table S1 and Figure 1a. They were investigated before, 2 and 5 years after RYGB. Presently we focused on first (n=50) and second examination (n=49) when there was a substantial bodyweight loss. Three had type-2 diabetes pre-surgery treated with metformin and/or diet only. Diabetes was absent following RYGB. Sixteen women had hypertension at baseline and treated with ACE- or angiotensin 2 receptor blockers, beta-blockers, thiazide diuretics and/or calcium channel antagonists; 9 women remained on antihypertensive treatment at two years follow up. Two women were on statins pre-surgery, one remained after surgery. All women received dietary instructions following surgery of a protein-rich diet for six weeks. Eating subsequently three small meals rich in protein and whole grains and four small snacks per day was advised. For additional studies we investigated 10 lean women (body mass index 20.4 – 24.6; mean 23.05 kg/m^2) and 9 women with obesity (body mass index 31.0 – 54.4; mean 40.47 kg/m^2). All were middle aged, apparently healthy and body weight stable. Methods for measurements of blood lipids, serum insulin and *in* vivo insulin sensitivity have been described in detail[16]. The study was approved by the local committee on ethics (Regionala Etikprövningsnämnden in Stockholm) and explained in detail to each participant who gave informed written consent.

Clinical measurements

All examinations took place at 8am after an instructed overnight fast. Anthropometric and clinical chemistry variables were determined as described[16,17]. Total fat mass was calculated by bioelectrical impedance analysis. A WAT needle biopsy from the abdominal subcutaneous region lateral to the umbilicus was obtained each time. The samples were rinsed in sodium chloride (9mg/mL) and portioned into two fractions, one 300mg sample was frozen in liquid nitrogen and stored for gene expression analysis. The second fraction was used for adipocyte isolation to determine fat cell size as described[55].

Cell culture

Human adipose derived stem cells (hADSC) were isolated from the subcutaneous WAT as described and used previously[56]. hADSC were cultured and passaged in Dulbecco's modified Eagle's medium (DMEM) with 1 g/L of glucose (31885-023, Gibco, 10% FBS (SV301060.03, GE Healthcare), FGF_2 (2.5 ng/ml) (Sigma-Aldrich), penicillin/streptomycin (100 U/ml) and maintained at 37ºC in a humidified gassed incubator at 5% CO_2. For adipocyte differentiation, hADSC were cultured in DMEM/Ham's F12 media (21765-029, Gibco) supplemented with 10 µg/ml transferrin (Sigma-Aldrich), 0.86 µM insulin (Sigma-Aldrich), 0.2 nM triiodothyronine (Sigma-Aldrich), 1 µM dexamethasone (Sigma-Aldrich), 100 µM isobutyl-methylxanthine (Sigma-Aldrich), and 1 µM rosiglitazone (Caymen Chemical). After three days, dexamethasone and isobutyl-methylxanthine were removed; after nine days rosiglitazone was removed. Knockdown of the target lncRNA (ADIPINT) was carried out on day 8 of differentiation (when the cells showed adipocyte features), using a Neon™ transfection system MPK5000 (Invitrogen) with 2 pulses of 20 ms at 1300 V. Antisense LNA GapmeRs (Qiagen) used for *ADIPINT* knockdown and control conditions are given in Supplementary Methods Table 1. For PC inhibition experiments, Sodium Oxalate (Sigma-Aldrich) was added two hours post-transfection. All hADSC analyses were performed at day 13 of differentiation apart from lipid synthesis on day 14. For RNA quantification, basal lipolysis, triglyceride content and lipid synthesis hADSC were cultured in 24-well plates at 2 x 10^5 cells/well. For bioenergetic quantification hADSC were plated on a Seahorse XF Microplate (Agilent) at 1.6 x 10^4 cells/well. For transcriptomics, quantitative proteomics and measurement of PC activity, hADSC were cultured in 6-well plates at 4 x 10^5 cells/well.

Gene expression analysis

Microarray analysis of coding genes in the WAT has been detailed[17]. Briefly, total RNA was extracted from frozen WAT with the RNeasy kit (Qiagen) and subjected to global transcriptome analysis using Clariom™ D arrays (Affymetrix) according to the manufacturer's instructions. The WT Plus Kit (Thermo Fisher) was used to amplify and biotinylate sense strand target cDNA before 5.5 µg was fragmented and hybridized to the arrays in a GeneChip Hybridization Oven 645 at 45°C for 16-18 h. Arrays were washed and stained in a GeneChip Fluidics Station 450 prior to scanning in a Affymetrix GeneChip Scanner 7. Microarray gene expression analysis in hADSC after *ADIPINT* knockdown was carried out as described above, apart from

that RNA was isolated using a NucleoSpin RNA Isolation Kit (Machery-Nagel). CEL files were preprocessed and analyzed using the Affymetrix Expression Console (version 1.4.1) and standard SST-RMA method. Affymetrix probe IDs were mapped to the FANTOM-CAT gene model[7], 54,980 probe sets mapped to 40,590 unique gene IDs. Qlucore Omics Explorer (http://www.qlucore.com) software was used to compare arrays as detailed previously[17]. Genes annotated 'lncRNA' were selected for analysis and a paired comparison was made across time points with the effect of sample eliminated. qRT-PCR analysis was carried out as described previously[9]. Probes targeting ADIPINT, PC, GAPDH, 18S, B2M, MALAT1, NEAT1 and MT-ND5 are listed in Supplementary Methods Table 2. The $^{\Delta\Delta}C_T$ method was used for normalization for all experiments apart from RNA analysis in whole of fractionated WAT where the $^{\Delta}C_T$ method was used. Either 18S or B2M were used as housekeeping controls in all experiments.

Fluorescence Microscopy

RNA-FISH assays for ADIPINT and immunofluorescence for PC was combined performed using the ViewRNA® ISH Cell Plus Assay Kit (Affymetrix) according to the manufacturer's instructions. Type 6 probes against ADIPINT were ordered from the same supplier. Briefly, hADSC were cultured in Millicell EZ SLIDE 4-well glass chambers (Merck Chemicals and Life Science AB). At day 13 of differentiation, the adipocytes were washed with phosphate buffered saline (PBS) and fixed in 4% paraformaldehyde for 20 min at room temperature. Following incubations with α-PC (PA5-50101) at 1:50 for 2 hours at room temperatures, the cells were incubated with Alexa Fluor® 568-conjugated secondary antibodies (A11011 , ThermoFisher) at 1:1000 for 1h at room temperature. Subsequently, probes were hybridized for 2 hours at 40°C. After hybridization and amplification steps with pre-amplifier, amplifier, and linked labelled probe, the probes were detected using Alexa® Fluor 650 dyes, according to the manufacturer's instructions. Cells were stained with 1:2500 BODIPY 493/503 and Hoechst 33342 for 20 minutes before mounting with ProLong Gold Antifade Mountant (ThermoFisher). Images were obtained with a Nikon spinning disk confocal microscope system (Nikon) equipped with a Nikon ECLIPSE Ti inverted microscope and a 1.4 NA 60x oil immersion objective (Nikon), under the control of NIS-Elements AR version 4 software.

Proteomic analysis

Cell pellets were solubilized with 100 µL of 8M urea and sonicated in a water bath for 10 min followed by further sonication using a VibraCell probe (Sonics & Materials, Inc.) for 40 s, with pulse 5/2, at 20% amplitude. Proteins were precipitated with 400 µL chilled acetone and incubated at -20°C overnight. Protein concentration was measured by BCA assay (ThermoFisher) after centrifugation (13,000 rpm) at +4°C for 20 minutes and solubilizing proteins with 10 µL of 8M urea and adding 10 µL ddH2O. 10 µg of protein in 253 µL of 133 mM ammonium bicarbonate (AmBic), pH 8 were sonicated in a water bath for 5 minutes and subjected to tryptic digestion following protein reduction in 5 mM dithiothreitol (Sigma) at 37°C for 60 minutes and alkylation in 15 mM iodoacetamide for 60 minutes at room temperature in the dark. Trypsin (sequencing grade, Promega) was added in an enzyme to protein ratio of 1:20 (5 µL of 0.1 µg/µL) and digestion was carried out overnight at 37°C. The digestion was stopped by adding formic acid at a final concentration of 5%. The samples then were cleaned on a C18 Hypersep plate with 40 µL bed volume (Thermo Scientific) and dried using a speedvac (MiVac, ThermoFisher).

Samples were dissolved in 70 µL of 50 mM triethylammonium-bicarbonate (TEAB), pH 8, and 40 µg of TMT-11 plex reagents (ThermoFisher) in 30 µL of dry acetonitrile were added. Samples were scrambled and then incubated at RT, 550 rpm for 2 hours. The reaction was stopped by adding hydroxylamine at a final concentration of 0.5% and incubated at RT with 550 rpm for 15 minutes. Individual samples were combined to one analytical sample and dried in a speedvac, followed by cleaning on a C18 StageTip and re-dried in a speedvac.

Chromatographic separation of peptides was performed on a 50 cm long C18 reversed phase EASY-spray column connected to an Ultimate 3000 UPLC system (ThermoFisher). The gradient was run for 120 minutes at a flow rate of 300 nL/minutes and was as follows: 2-26% of buffer B (2% acetonitrile, 0.1% formic acid) for 110 minutes, up to 35% of buffer B for 10 minutes and up to 95% of buffer B for 2 minutes.

Mass spectra were acquired on an Orbitrap Fusion tribrid mass spectrometer (ThermoFisher) in 375 m/z to 1600 m/z at resolution of R=120,000 (200 m/z) for full mass, targeting 4x105 ions, followed by data-dependent higher-energy collisional dissociation (HCD) fragmentations from precursor ions with a charge state 2+ to 7+ in 3 s cycle time. The tandem mass spectra were acquired with a resolution of R=60,000, targeting 5x104 ions, setting quadrupole isolation width to 1.6 m/z and normalized collision energy to 30%.

The raw files were imported to Proteome Discoverer v2.3 (ThermoFisher) and analyzed using the SwissProt protein database with Mascot v 2.5.1 (MatrixScience Ltd) search engine. Parameters were chosen as follows: up to two missed cleavage sites for trypsin, peptide mass tolerance 10 ppm, 0.02 Da for the HCD fragment ions. Carbamidomethylation of cysteine was specified as a fixed modification, whereas oxidation of methionine and deamidation of asparagine was defined as variable modifications.

hADSC lipid metabolism

Basal (spontaneous) triglyceride hydrolysis (lipolysis) was quantified through medium glycerol concentration after three days incubation as described[57]. 50 µL of differentiation media was collected and added to 450 mL of resuspended ATP reagent (10 µL purified glycerokinase (Sigma-Aldrich) and 10 µL ATP Reagent SL (Biotherma) in 0.05 M Tris buffer). The decay in luminescence was measured over one minute and compared to a glycerol standard curve. Medium not exposed to cells was used as background. Cellular triglyceride content was determined using a triglyceride quantification kit MAK266 (Sigma-Aldrich). Each well was washed in PBS twice and cells were lysed in 5% NP-40 in dH20. Florescence was measured at 590 nm on an Infinite M200 microplate reader (Tecan) and background was subtracted using the same volume of cell lysate minus addition of the lipase enzyme as suggested by the manufacturer. A triglyceride standard curve was used to determine concentration. The lipid synthesis rate was measured through incorporation of [$^{1\text{-}14}$C]-acetic acid (Perkin-Elmer) into acylglycerol lipids as described previously[58]. On day 13 of differentiation cells were cultured in DMEM media with no insulin, 10 µg/ml transferrin, 0.2 nM triiodothyronine and 1 µM glucose overnight. The following day, cells were cultured for 3 hours in DMEM media containing 2 mM glucose, 10 mM HEPES, 0.2% BSA, 2 mM acetate and 1 mCi [$^{1\text{-}14}$C]-acetic acid with or without 100nM insulin. Cells were scraped in PBS with 0.1% SDS and radioactivity determined on a Tri-Carb 4910 TR scintillation counter (Perkin-Elmer).

hADSC energy metabolism

Bioenergectis were quantified using a XF96 Seahorse Extracellular Flux Analyzer (Agilent) as per manufacturers instructions. The Seahorse Glycolysis Stress Test Kit (Agilent) was used to assess OCR and ECAR at basal then after Glucose, Oligomycin and 2-deoxyglucose treatment. All concentrations used were as recommended by the manufacturer. Basal OCR and ECAR were carried out in medium supplemented

with 2 mM glutamine. OCR and ECAR for each well was normalized to cell number by Hoechst 33342 staining of nuclei before counting using a CellInsight CX5 High Content Screening Platform (Fisher Scientific).

Targeted RNA identification using orthogonal organic phase separation (TROOPS)

Purification of the RNA-bound proteome was performed using orthogonal organic phase separation (OOPS) as described[23], and adapted by us for targeted pulldown of a specific RNA (TROOPS). hADSC plated at 3 x 10^6 cells in 15 cm^2 cell culture dishes were proliferated for 3 days (reaching ~90% confluence) before initiating differentiation. At day 13, cells were washed twice in ice-cold PBS and crosslinked at 254 nm (0.15 J/cm^2) on a UV Crosslinker 2400 (Stratagene). Cells were immediately scraped in 1mL Trizol (Invitrogen), transferred to a new 2 mL tube and left to stand for at least 5 minutes to allow unstable RNA-protein interactions to dissociate. 225 µL of chloroform was added to each tube, which was vortexed and spun for 15 minutes at 16,100 x g at 4ºC. The upper aqueous phase (containing free RNA) and organic phase (containing free protein) was removed using a 25G needle syringe. The interphase was washed in 1 mL Trizol followed by 200 µL chloroform twice, each time vortexed and spun before removal of aqueous and organic phases. Nine volumes of EtOH was added to the interphase and the sample stored at -20ºC for 30 minutes. Following incubation, the interphase was pelleted by centrifugation at 20,000 x g for 20 minutes at 4ºC, the EtOH removed, the pellet gently washed in 80% EtOH and spun at 20,000 x g for 15 minutes at 4ºC; this wash step was performed twice. The pellet was resuspended in 500 µL of 50 mM Tris-Cl (pH 7.0), 10 mM EDTA and 1% SDS with 1 mM PMSF, 0.1 U/ µL SUPERase-In™ RNase Inhibitor (Invitrogen) and cOmplete Mini EDTA-free protease inhibitor cocktail (Roche). Two re-suspended pellets were pulled and sonicated using a Bioruptor® Pico (Diagenode) for 15 cycles (30 seconds on, 45 seconds off) with sonication beads. 1.75 mL of lysate (equivalent to 3.5 x 15 cm^2 culture dishes) was used per replicate in each TROOPS experiment. 15 µL of lysate was taken for protein and RNA input samples. Probe design and hybridization was modified from the ChirP-MS protocol[21]. For targeted pulldown, 24 biotinylated short oligos (Biosearch Technologies) were designed against *ADIPINT* and split into two pools termed odd and even. Each probe was numbered sequentially from 5' to 3', odd numbered probes were split into one pool and even numbers to another. A probe set designed against *Lac Z* mRNA was used as a control for non-specific probe

interactions and odd and even probes added in the presence of RNase A (20 µg/mL) (Sigma-Aldrich) to control for the RNA independent pulldown of the target probes. All probe sequences are given in Supplementary Methods Table 3. 3.5 mL hybridization buffer (50 mM Tris-Cl (pH 7.0), 750 mM NaCl, 1% SDS, 1 mM EDTA, 15% formamide, 1 mM PMSF, 0.1 U/µL SUPERase-In™ RNase Inhibitor and cOmplete Mini EDTA-free protease inhibitor cocktail) was added to each lysate and 250 pmol targeting probes. Hybridization was carried out overnight at 37ºC with rotation. 500 µL of pre-washed MyOne™ Streptavidin C1 Dynabeads™ (Invitrogen) were added the following day for 2 hours at 37ºC with rotation. Beads were extracted on a Dynamag-15 magnetic strip and washed 5 times in 300mM NaCl, 30mM sodium citrate, 0.5% SDS and 1 mM PMSF. After final wash, 10% was taken for RNA purification and 90% for protein identification using mass-spectrometry. RNA bead samples were re-suspended in Proteinase K buffer (10 mM Tris-Cl (pH 7.0), 100 mM NaCl, 1 mM EDTA, 0.5% SDS) with 5% (v/v) Proteinase K (20 mg/mL) (Ambion) added and incubated at 50ºC for 45 minutes with rotation. Samples were boiled at 95ºC for 10 minutes and cooled on ice before addition of 1 mL Trizol and RNA purification using the miRNeasy Mini Kit (Qiagen). qRT-PCR analysis of *ADIPINT* as well as two non-targeted abundant RNAs *GAPDH* and *18S* to assess pulldown efficiency. Protein bead samples were re-suspended in 22uL of PBS with 1uL RNase A (20 µg/mL), 1uL RNase H (10 U/µL) and 1uL cOmplete Mini EDTA-free protease inhibitor cocktail supplemented in and incubated for 45 minutes at 37ºC. 5 µL of Laemmli Sample Buffer was added to each sample before heating to 95ºC for 10 minutes. Samples were run onto an SDS-PAGE gel, zinc stained to confirm protein loading and individual lanes were cut for MS-analysis or gel was transferred to a PVDF membrane for Western blot analysis.

For MS-analysis, gel pieces were washed with 0.2M ammonium bicarbonate (AmBic) containing 50% acetonitrile. Proteins were reduced with 20 mM dithiothreitol (DTT) in 100 mM AmBic for 60 minutes at 37°C, followed by alkylation with 55 mM iodoacetamide in 100 mM AmBic for 20 minutes at 25°C and digested with 0.2 µg trypsin (sequencing grade) in 0.2 M AmBic overnight at 37°C. The tryptic peptides were acidified with formic acid and extracted twice using 0.1% formic acid in 50% and 100% acetonitrile, respectively. The solutions were dried and the peptides were cleaned up on C-18 Stage Tips (ThermoFisher).

The reconstituted peptides in solvent A (0.1% formic acid in 2% acetonitrile) were separated on a 50 cm long EASY-spray column (ThermoFisher) connected to an Ultimate-3000 nano-LC system (Thermo Scientific) using a 60 minutes gradient from 4-26% of solvent B (98% AcN, 0.1% formic acid) in 55 min and up to 95% of solvent B in 5 minutes at a flow rate of 300 nL/minutes. Mass spectra were acquired on a Q Exactive HF Orbitrap mass spectrometer (ThermoFisher) in 350 m/z to 1600 m/z at resolution of R=120,000 (at 200 m/z) for full mass, followed by data-dependent higher energy collisional dissociation (HCD) fragmentations from the 17 most intense precursor ions with a charge state 2+ to 7+. The tandem mass spectra were acquired with a resolution of R=30,000, targeting 2x105 ions, setting quadrupole isolation width to 1.4 m/z and normalized collision energy to 28%.

Acquired raw data files were analyzed using the Mascot search engine v.2.5.1 (Matrix Science Ltd). Maximum of two missed cleavage sites were allowed for trypsin, while setting the precursor and the fragment ion mass tolerance to 10 ppm and 0.02, respectively. Carbamido-methylation of cysteine was specified as a fixed modification. Dynamic modifications of oxidation on methionine, deamidation of asparagine and glutamine and acetylation of N-termini were set. Initial search results were filtered with 5% FDR using Percolator to recalculate Mascot scores.

RNA immunoprecipitation (RIP)

hADSC were plated in 15 cm^2 cell culture dishes, differentiated until day 13 and UV-crosslinked as described for TROOPS using one 15cm^2 cell culture dish per condition. Immediately there after cells were scraped in 1 mL RIP lysis buffer (50 mM Tris-Cl (pH 7.0), 150mM NaCl, 10 mM EDTA, 1% Triton X-100 ,1mM DTT, 0.1 U/µL SUPERase-In™ RNase Inhibitor and cOmplete Mini EDTA-free protease inhibitor cocktail). Samples were passed through a 23 G syringe 20 times and spun at 12,000 x g for 10 minutes at 4ºC. The lysate was removed and cleared with 30 uL of Pierce™ Protein A/G magnetic beads (Thermo Scientific) for 30 minutes on rotation at room temperature. Magnetic beads were removed, and the sample spun once more at 12,000 x g for 10 minutes at 4ºC and lysate transferred to a fresh tube. Seven µg of rabbit pyruvate carboxylase (PA5-50101, ThermoFisher) or rabbit IgG (PP64B, Millipore) antibody was incubated with the lysate overnight at 4ºC with rotation. The following day 1:10 w/v Protein A/G beads were added to each sample and incubated for 3 hours at 4ºC with rotation. Magnetic beads were extracted using a

Dynamag-2 magnetic strip and washed for 5 minutes five times in RIP lysis buffer on rotation at room temperature. Bead samples were processed for RNA purification as described for TROOPS.

Gel filtration analysis

ADIPINT or ADIPINT anti-sense cDNA was cloned out of a plasmid containing the full length cDNA sequence for ADIPINT transcript 2 (MICT00000363691.1) using KOD Hot Start Polymerase (Sigma-Aldrich) as previously described[59]. The PCR product was confirmed by size and EcoRI-HF (NEB) restriction digest, bands were excised from the agarose gel and purified using the NucleoSpin Gel and PCR Clean-up kit (Machery-Nagel). The RNAMaxx Transcription Kit (Agilent) was used as per manufacturers instructions to synthesize RNA, with 1 µg of template DNA product used per reaction. The reaction was carried out for two hours at 37ºC before RNA was purified using the NucleoSpin RNA Isolation Kit (Machery-Nagel). For RNA-PC binding, RNA was added to purified bovine PC (0.3 µg/µL Sigma-Aldrich) in a 110 uL reaction containing 10mM HEPES (pH 7.3), 20mM KCl, 1mM $MgCl_2$, 1mM DTT, 5% Glycerol and 0.1 U/µL SUPERase-In™ RNase Inhibitor and left at room temperature for 30 minutes. To establish the RNA UV absorption peak ADIPINT RNA was added to PC at a 1:1 molar ratio. For experiments comparing ADIPINT to ADIPINT anti-sense, RNA was added to PC at a 0.25:1 molar ratio and DTT was omitted from the reaction. 100 µL of each reaction was then injected to a Superose® 6 Increase 10/300 GL column (Cytiva) using the Äkta go system (Cytiva) with the running buffer (pH 7.3), 20mM KCl, 1mM MgCl2, 5% Glycerol and 0.01 U/µL SUPERase-In™ RNase. 250 µL of the indicated peak fractions (280 nm) from the gel filtration were collected and concentrated using Vivaspin® 500 (Sartorius) centrifugal concentrators (100K MWCO, PES) for western blot analysis.

Cellular fractionation

For fractionation of the nuclear and cytoplasmic compartments the RNA subcellular isolation kit (25501, Active Motif) was used as per manufactures instructions. Briefly hADSC cells cultured in 1 x $15cm^2$ cell culture dish was differentiated to day 13 and washed in cold PBS before being scraped in complete lysis buffer provided by the kit. Cells were passed through a 23G syringe 10 times and left for 20 minutes on ice to allow for sufficient lysis. The lysate was split in two, one aliquot for total RNA and the other for nuclear

and cytoplasmic RNA isolation. The samples were washed and loaded onto the columns as instructed. *GAPDH* and *NEAT1* RNA were used to validate the cytoplasmic and nuclear fractions, respectively.

For fractionation into mitochondrial/membrane, cytoplasmic and lipid droplet compartments, hADSC cells cultured in 1 x 15cm^2 cell culture dish were differentiated to day 13 and washed in cold PBS twice before being scraped in 750 µL homogenization buffer (20 mM Tris-HCl pH 7.4, 250 mM sucrose, 1 mM EDTA, 0.1 U/µL SUPERase-In™ RNase Inhibitor and cOmplete Mini EDTA-free protease inhibitor cocktail). Cells were passed through a 23G syringe 10 times and spun at 1,000 x g for 10 minutes at 4ºC removing nuclei and intact cells. The lysate was transferred to a fresh Eppendorf and spun at 20,000 x g for 40 minutes at 4ºC to pellet the mitochondrial/membrane fraction and lysate transferred to an ultracentrifugation tube (344057, Beckman) and mixed 1:1 with 50% OptiPrep Density Gradient Medium (D1556, Sigma-Aldrich) diluted in homogenization buffer. OptiPrep gradient solutions of 22, 16, 12, 8, 5, 2, and 0% were layered on top. Samples were spun overnight at 150,000 x g at 4ºC in a SW55 Ti swinging bucket rotor (Beckman-Coulter). Fractions were collected with a pipette and RNA/proteins were precipitated using the Wessel and Flügge method[60]. Each sample was split into two before precipitation, RNA samples were resuspended in 750 µL Trizol and subject to RNA isolation as described above. Samples for protein analysis were resuspended in RIPA Lysis and Extraction Buffer (89900, ThermoFisher) with a final concentration of 2% SDS. Western blot analysis was carried out as described above with the following antibodies used to stain for PLIN1 (D1D8, CST, 1:1000), GAPDH (14C10, CST, 1:1000), H3 (07-473, Millipore, 1:20000), and TOM20 (D8T4N, CST, 1:1000). All blots were incubated with the primary antibody overnight at 4ºC and the rabbit/mouse secondary antibody α-rabbit IgG, HRP-linked antibody (7074, CST) for 1 hour at room temperature.

Pyruvate carboxylase (PC) activity assay

PC activity was measured using the coupled enzyme reaction with malate dehydrogenase as described[23] with the following modifications. Cells were rinsed in cold PBS twice before being scraped in 180 µL assay buffer (10 mM HEPES (pH7.4), 250 mM sucrose, 2.5 mM EDTA, 2mM cysteine and 0.02% BSA). Scraped cells were passed through a 23 G needle 10 times and sonicated using a Bioruptor® Pico for 15 cycles (30 seconds on, 45 seconds off) with no sonication beads added. Sonicated samples were spun at 11,000 x g for

10 minutes at 4ºC and 20 µL of lysate was saved for total PC quantification using western blot. Briefly, 5X Laemmli Sample Buffer was added to each sample, heated at 90ºC for 7 minutes, before loading onto a 4-12% SDS-PAGE gel. After running, the protein was transferred to a PVDF membrane using the Trans-Blot® Turbo™ Transfer System (Bio-Rad) as per manufacturer's instructions. The membrane was blocked and incubated with rabbit pyruvate carboxylase (PA5-50101) or house-keeping α-tubulin (2144, CST) antibody overnight at 4ºC. The following day the membrane was washed with TBS-Tween 20 (0.1%) and incubated with α-rabbit IgG, HRP-linked antibody (7074, CST) for 1 hour at room temperature. The membrane was washed in TBS-Tween 20, and the protein signal developed using the ECL™ Select Western Blotting Detection Reagent (GE Healthcare). Bands were visualized on a ChemiDoc MP Imaging System (Bio-Rad). Image J software was used to measure densitometry of PC and α-tubulin bands. 30 µL of the remaining lysate was added to 225 µL of PC activity buffer (80mM Tris-Cl (pH 8.0), 2 mM ATP, 8 mM sodium pyruvate, 21 mM $KHCO_3$, 9 mM $MgSO_4$, 0.16 mM acetyl-CoA, 0.16 mM NADPH and 30 units of purified malate dehydrogenase (LMDH-RO Roche)). The absorbance at 340 nm (Absorbance of NADH) is read immediately, every 15 seconds for 4 hours on a Varioskan™ LUX multimode microplate reader (Thermo Scientific). PC activity was calculated as the time taken to reach 50% completion of the reaction ($½V_{max}$) using the nonlinear regression method with the Michaelis-Menten equation applied in GraphPad Prism 8.0. The relationship between PC concentration and $½V_{max}$ was determined as linear ($R^2 = 0.9204$) by titrating down GapmeR NC transfected lysate and running both PC western blot and activity assay on the same sample (Extended Data Fig. 6). Each $½V_{max}$ and PC densitometry value was normalized to the average value for all the samples in that experiment to allow comparison between experiments ran on different days. For measurement in the mitochondrial fraction, cells were scraped in assay buffer and fractionated as stated above. The mitochondrial pellet was resuspended in assay buffer and activity measured. For measurement in WAT, 100 mg pieces were incubated on dry ice with 2 x 5 mm ball bearing before 1 mL of assay buffer was added and tissue lysed using a Tissue Lyser LT (Qiagen) at 50 oscillations/second for 10 minutes. 30 µL of lysate was saved for total PC quantification using western blot. The PC activity was then determined as stated above. Another 100 mg piece from the same biopsy was incubated on dry ice with 1 x 5 mm ball bearing and lysed in 1 mL Trizol at oscillations/second for 5 minutes and subjected to RNA isolation as stated above.

PC Immunoprecipitation

hADSCs grown in 1 x 15 cm^2 dishes per condition were washed twice in cold PBS and scraped in RIP lysis buffer without 1 % Triton X-100 or 1 mM DTT. The mitochondrial/membrane fraction was isolated as stated above and resuspended in RIP lysis buffer without 1 mM DTT. The immunoprecipitation was carried out as stated for the RIP with the following modifications. 3 ug of PC antibody (16588-1-AP, ProteinTech) or rabbit IgG antibody was incubated with the lysate overnight at 4oC with rotation. The following day 30 uL of Protein A/G beads were added to each sample and incubated for 30 minutes with rotation. Magnetic beads were extracted using a Dynamag-2 magnetic strip and washed for 5 minutes five times in Pierce™ IP lysis buffer (ThermoFisher) on rotation at room temperature. Bead samples were processed for mass-spectrometry as described for TROOPS.

Statistical analyses

GraphPad Prism v8.0 was used for all statistical comparisons unless otherwise stated. The specific statistical test used for each comparison mentioned in the figure legend. All data are expressed as mean ± S.D for experiments with sample size $n < 6$ and S.E.M when n was higher. All n represent biologically independent experiments. For ANOVA, Dunnett post-test was used for comparisons of all samples to a particular sample and Holm-Sidak was used for comparisons of all samples to one another. Comparisons between *ADIPINT* knockdown and control samples in microarray and proteomic studies were carried out using the Bioconductor R package Limma[61]. An FDR ≤ 0.05 was used to select for significant genes and FDR ≤ 0.1 for proteins in all comparisons. Pearson correlation was used to assess significance between the change in *ADIPINT* expression versus weight/adipocyte cell volume and *ADIPINT* versus PC mRNA expression at all time points. A p-value of ≤ 0.05 was considered significant.

Data Availability

All data that support the findings is available on request to the corresponding authors within reason. Material and correspondence requests should be made to the corresponding authors

Acknowledgements

The expert technical assistance of Katarina Hertel, Ana Maria Suzuki and Thais De Castro Barbosa is greatly acknowledged. This study was supported with grants from the Swedish Research Council, Novo Nordisk Foundation, the Strategic Diabetes Research Program at Karolinska Institutet, EMIF (Stockholm County) and the European Research Council (ERC) Synergy Grant SPHERES (agreement No. 856404) under the European Union's Horizon 2020 research and innovation programme (erc-spheres.univ-tlse3.fr). A Human Frontier

Science Program grant ´(RGY0074/16) awarded to C.M. The China Scholarship Council (CSC) program awarded to Z.W. AG Kerr, KHM Kwok and A Ludzki were sponsored by the Novo Nordisk Postdoctoral Fellowship program at Karolinska Institutet. Protein identification, quantification, in-gel digestion, mass spectrometric analysis and database searches for protein identification was carried out at the Proteomics Biomedicum core facility, Karolinska Institute, Stockholm. (https://ki.se/en/mbb/proteomics-biomedicum). RNA sequencing and microarray was carried out at BEA core facility at Karolinska Institute, Stockholm (https.bea.ki.se). We thank the Live Cell Imaging facility, Karolinska Institutet , Stockholm (https://ki.se/en/bionut/welcome-to-the-lci-facility) for microscopy imaging analysis.

Author Contributions

AGK, HG and PA planned the study, designed experiments and analyzed the data. AKG, HG, KHMK and AL performed experiments. AGK and HG developed TROOPS and DL developed the lipid synthesis assay. ZW and CM planned and performed the gel filtration experiments. MB advised and planned Seahorse experiments. PA recruited and phenotyped the clinical cohorts. ID provided microarray data on WAT. PA, AKG and HG wrote the first version of the paper. All authors contributed to further writing and approved the final version.

Extended Data

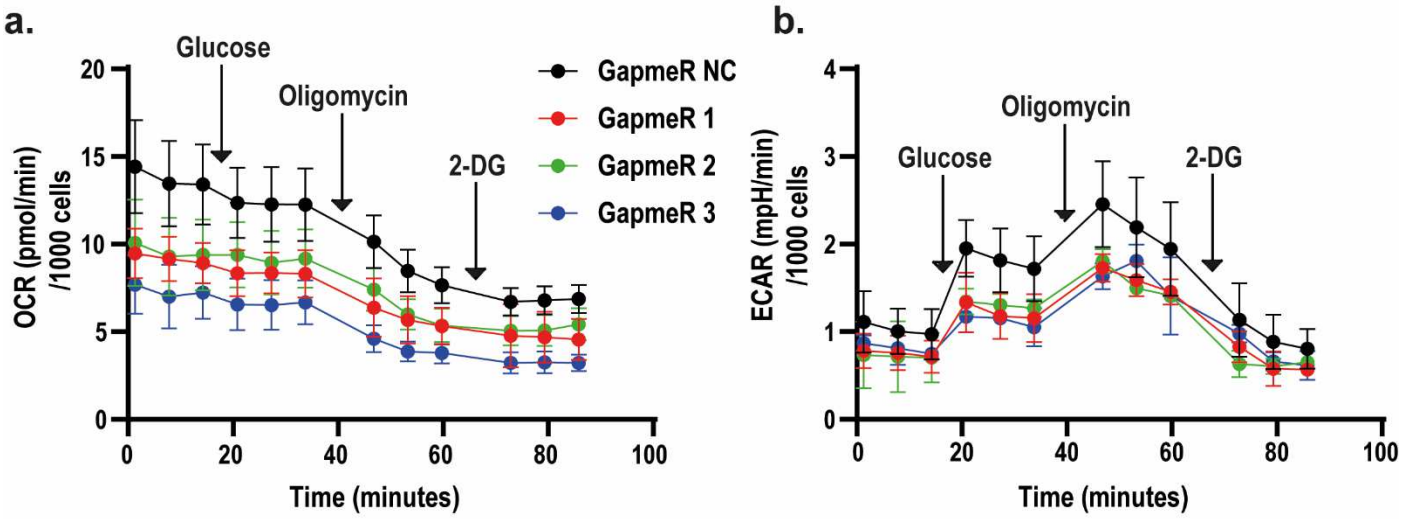

Extended Data Figure 1. Knockdown of ADIPINT decreases the aerobic and anaerobic respiration rate in hADSC.
a ADIPINT was knocked down using GapmeRs 1-3 and the oxygen consumption rate (OCR) and **b** extracellular acidification rate (ECAR) was measured at basal and then after glucose, oligomycin and 2-deoxyglucose treatment as indicated. GapmeR NC cells were used as a control. n = 3-5 per group. Error bars are SD.

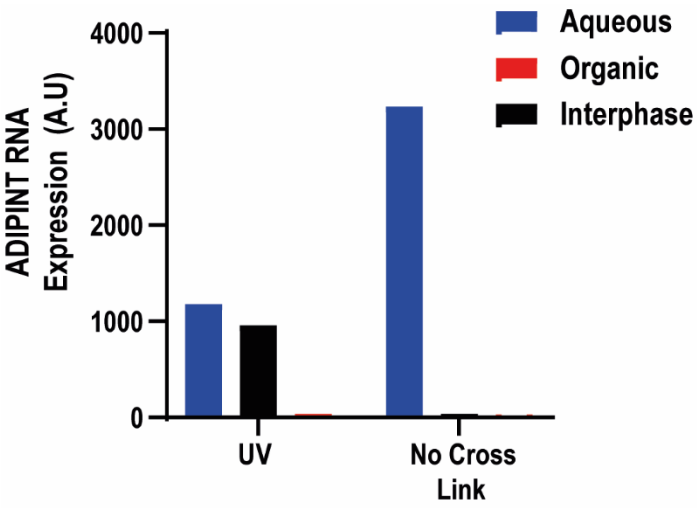

Extended Data Fig. 2: After UV crosslinking ADIPINT RNA enriches in the interphase
hADSC cells underwent UV crosslinking before collection in Trizol. After Trizol-chloroform seperation the aqueous and organic phase was collected. The interphase was subjected to two further rounds of Trizol-chloroform speration before collection. As a control uncrosslinked cells were used. ADIPINT expression was analyzed in each fraction and a shift into the interphase was seen after UV crosslinking.

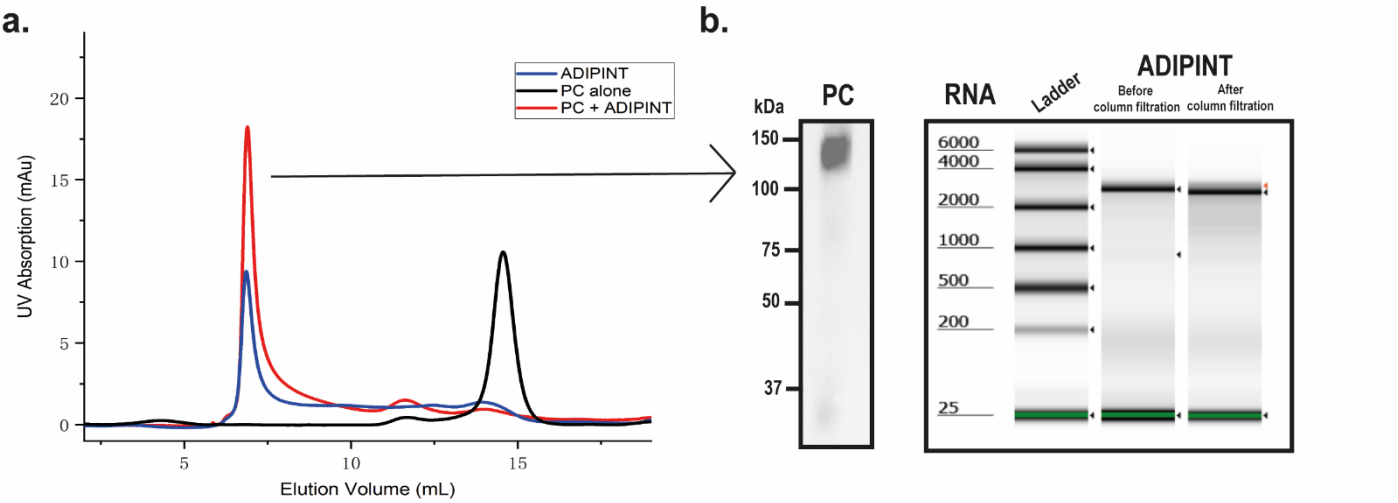

Extended Data Fig. 3: ADIPINT and PC elute in the same fraction after size seperation with a Sepharose column
a. Purified PC (black), purified ADIPINT (blue) and PC with ADIPINT were injected onto a Sepharose column and UV absorbtion measured. PC alone gave a peak at 14.56 mL (termed PC elution) and ADIPINT a peak at 6.87 mL (termed RNA elution). **b** The peak at 6.87 mL for the PC with ADIPINT injection was collected for protein (to the left) and RNA analysis. Western blot analysis revealed PC protein was present in the RNA elution peak alongside ADIPINT (to the right). ADIPINT before injection onto the column was run alongside ADIPINT recovered after column filtration demonstarting ADIPINT remained intact.

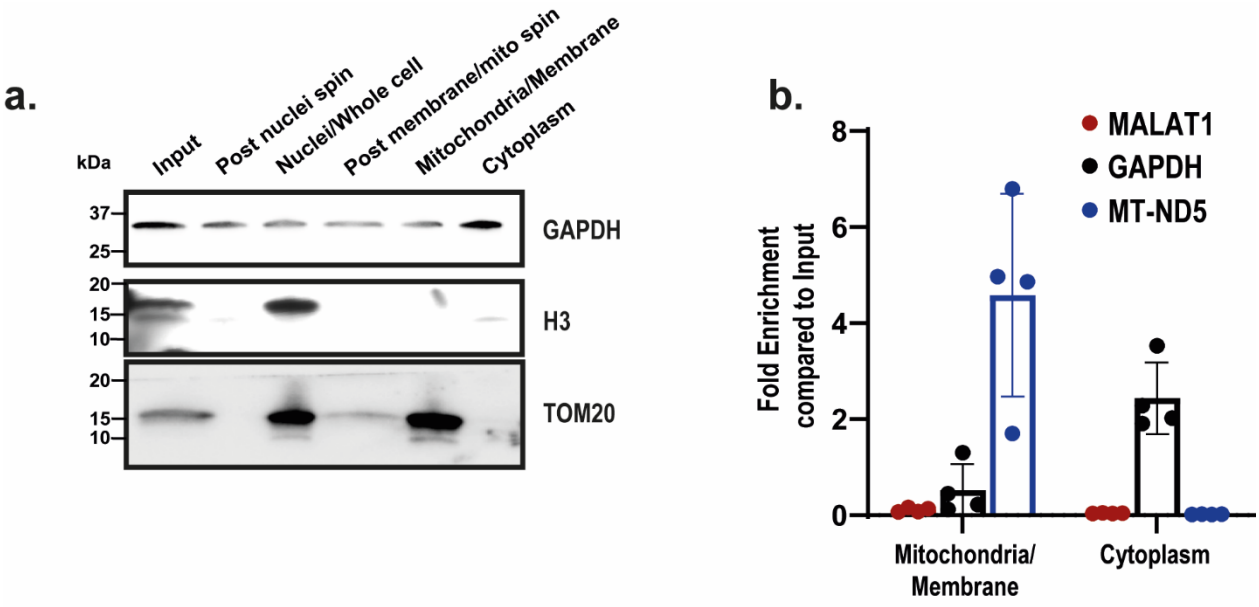

Extended Data Fig. 4: Ultracentrifugation of hADSC can enrich mitochondrial and cytoplasmic localised proteins in respective fractions

a. Western blot analysis of GAPDH (cytoplasmic), H3 (nuclear) and TOM20 (mitochondrial bound) proteins after ultracentrifugation. Nucleus was not purified. Post nuclei and post membrane refer to the lysate after respective spins to remove nuclear and membrane/mitochondria proteins. GAPDH and H3 were stained on the same blot after cutting at respective Mw. TOM20 was stained on a seperate blot. **b**. qRT-PCR analysis of MALAT1 (nuclear), *GAPDH* (cytoplasmic) and *MT-ND5* (Mitochondrial encoded) RNA in the same fractions western blot anlaysis was carried out in **a**.

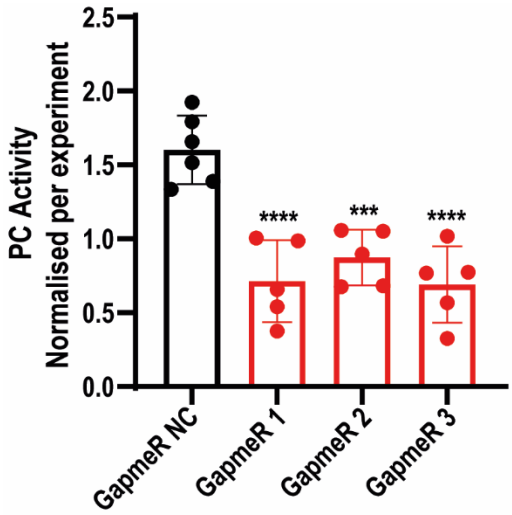

Extended Data Fig. 5 Pyruvate carboxylase activity is decreased after ADIPINT knockdown

PC activity assesed by the time to reach 50% completion for the reaction (seconds) is normalised to the average time across all conditions for each experiment and plotted. GapmeR 1, 2 and 3 targeting ADIPINT significantly decreased PC activity. One-way ANOVA with Dunnett post-test comparing each GapmeR to GapmeR NC was used to assess significance. Each data point represents an individual experiment, mean is plotted and error bars are SEM. *** < 0.001, **** < 0.0001.

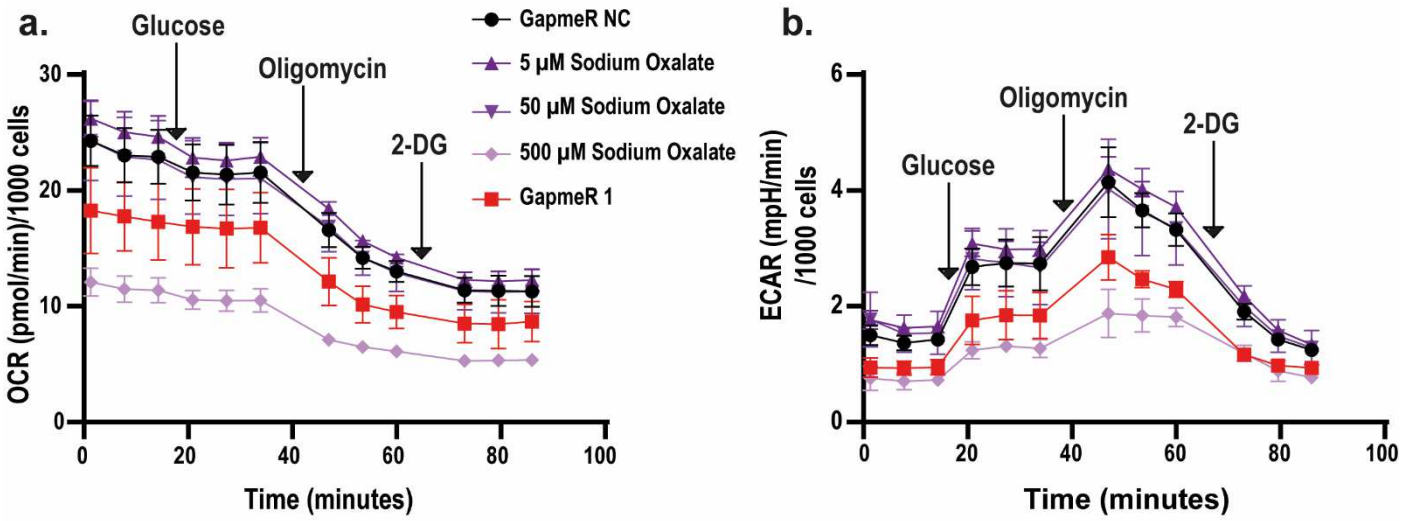

Extended Data Figure 6. Inhibition of pyruvate carboxylase decreases the aerobic and anaerobic respiration rate in hADSC.
a Sodium Oxalate (5-500 µM) was used to inhibit pyruvate carboxylase and the **a** oxygen consumption rate (OCR) and **b** extracellular acidification rate (ECAR) was measured at basal and then after glucose, oligomycin and 2-deoxyglucose treatment as indicated. GapmeR NC cells were used as a control and GapmeR 1 treated cells used as a positive control for reductions in OCR and ECAR. n = 3 per group. Error bars are SD.

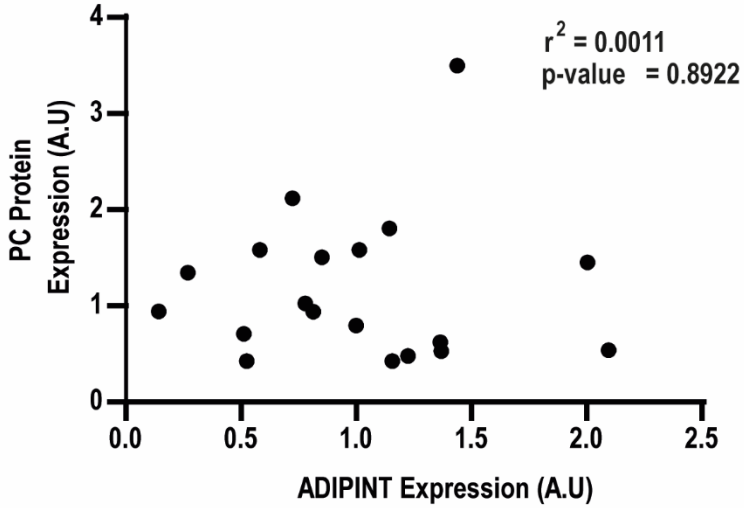

Extended Data Fig. 7 PC protein expression in WAT from lean and obese patients correlated with ADIPINT expression
PC protein expression from the lean and obese patients is plotted against ADIPINT expression measured in the same sample. No significant correlation was observed. Each data point represents one individual patient. Linear regression was used to assess significance.

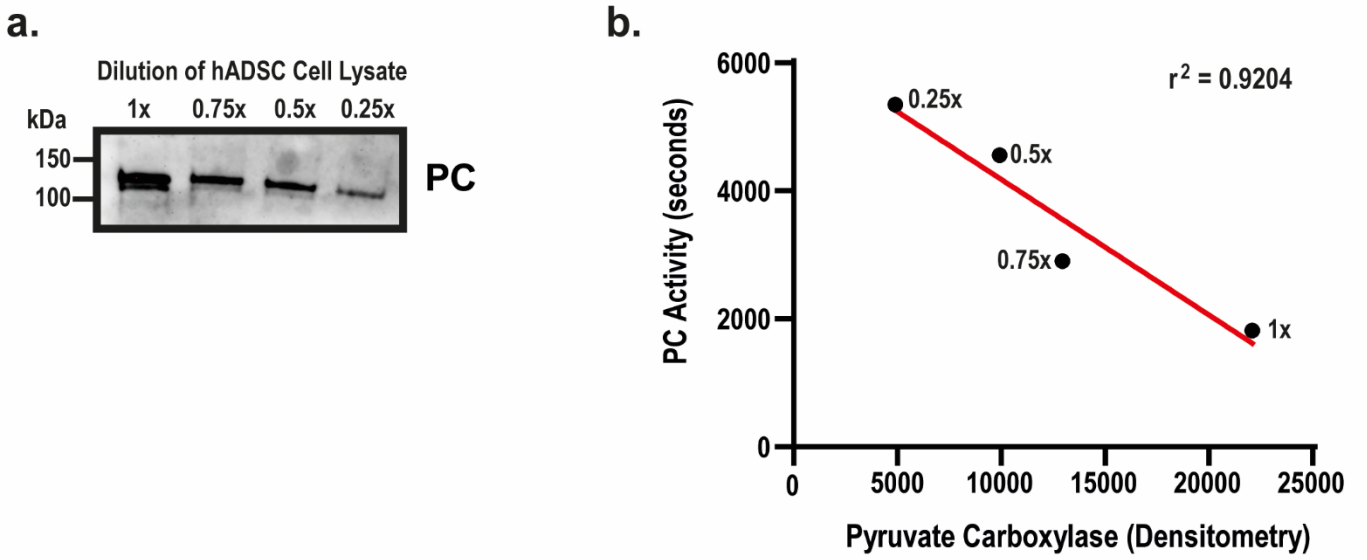

Extended Data Fig. 8 Pyruvate carboxylase protein expression and enzymatic activity share a linear relationship

a. Western blot analysis of PC after serial dilution of hMADSC cell lysate from 1x to 0.25x. **b**. PC activity (representing the time taken for 50% of the PC activity assay to be completed) for each dilution of hMADSC cell lysate plotted against the PC protein expression as shown in **a**.

Supplementary Files

This is a list of supplementary files associated with this preprint. Click to download.

- ADIPINTManuscriptSupplementaryTablesv2.xlsx
- ADIPINTManuscriptSupplementaryMethodsTables.xlsx